

Title	Characterization, Synthesis and Catalysis of Hydrotalcite-related Materials for Highly Efficient Materials Transformations
Author(s)	Nishimura, Shun; Takagaki, Atsushi; Ebitani, Kohki
Citation	Green Chemistry, 15(8): 2026-2042
Issue Date	2013-06-18
Type	Journal Article
Text version	author
URL	http://hdl.handle.net/10119/12087
Rights	Copyright (C) 2013 Royal Society of Chemistry. Shun Nishimura, Atsushi Takagaki, Kohki Ebitani, Green Chemistry, 15(8), 2013, 2026-2042. http://dx.doi.org/10.1039/C3GC40405F - Reproduced by permission of The Royal Society of Chemistry
Description	

Characterization, Synthesis and Catalysis of Hydrotalcite-related Materials for Highly Efficient Materials Transformations

Shun Nishimura ^a, Atsushi Takagaki ^b and Kohki Ebitani ^{*a}

^a School of Materials Science, Japan Advanced Institute of Science and Technology (JAIST), 1-1 Asahidai, Nomi, 923-1292, Japan

^b Department of Chemical System Engineering, School of Engineering, The University of Tokyo, 7-3-1 Hongo, Bunkyo-ku, Tokyo, 113-8656, Japan

Abstract

This review is intended to introduce recent progresses in characterization, syntheses and catalysis of hydrotalcite (HT) and HT-related materials. NMR, in situ neutron diffraction and TG-DTA techniques have been used to determine local structure and structural changes of HT. Various synthetic methods to control morphology of HT are introduced together with the crystal formation mechanism. Preparation methods of magnetic HTs are also included. The HT acts as heterogeneous base catalyst for efficient transformations of organic compounds such as synthesis of glycerol carbonate, transesterification of oils (biodiesel production) and carbon-carbon bond formations. The HT has been also used as a support for immobilizing various metal species (Ru, Pd, Ag, Au, Pt, Cu, V, Mn...) which enables highly selective organic reactions such as dehydrogenation of alcohols and deoxygenation of epoxides. Cooperative actions between basic sites of the HT surface and supported metal species are introduced. It is also shown that the HT can work together with other solid acid and metal catalysts to promote sequential reactions in one-pot manner, which gives us very important methodology for environmentally-benign synthesis of value-added chemicals especially from biomass-derived compounds.

1. Introduction

Hydrotalcite (HT) is a layered anionic clay denoted as $[M^{2+}_{1-x}M^{3+}_x(OH)_2]^{x+}A^{n-}_{x/n} \cdot mH_2O$, where M^{2+} and M^{3+} are di- and trivalent metal ions, and A^{n-} is the interlayer anion (Figure 1A).^{1,2} Anionic species such as CO_3^{2-} , NO_3^- , F^- and Cl^- are located within the interlayer galley due to the charge compensation of the positively charged Brucite layer, $[M^{2+}_{1-x}M^{3+}_x(OH)_2]^{x+}$. Water is also present in the interlayer galley which forms hydrogen-bond to the Brucite layers. $M^{3+}/(M^{2+} + M^{3+})$ ratio typically varies between 17 and 33%. A most widely used HT is Mg-Al type, *i.e.* $Mg_6Al_2(OH)_{16}CO_3 \cdot nH_2O$. The identical chemical formula is found for natural mineral HT.

The HT has attracted much attention due to the following characteristics:³⁻⁷ (i) adsorption capacity; (ii) cation-exchange ability of the Brucite layer; (iii) anion-exchange ability of the interlayer space; and (iv) tunable basicity of the surface. To control these properties of the HT, various synthetic methods have been developed and applied as a heterogeneous base catalyst and metal support for highly efficient liquid-phase organic transformations including one-pot synthesis and utilization of biomass-derived materials for *Green & Sustainable Chemistry*. In this review, the authors intend to survey recent progresses in characterization, syntheses and liquid-phase catalysis of HT and HT-related materials.

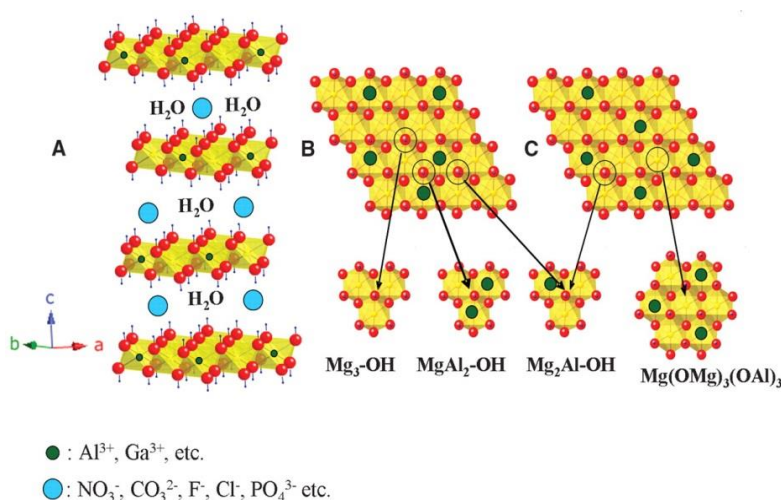


Figure 1 (A) A polyhedral representation of the LDH [layered double hydroxide] structure showing the metal hydroxide octahedral stacked along the crystallographic *c* axis. Water and anions are present in the interlayer region. Each hydroxyl group (dark blue) is oriented toward the interlayer region and may be hydrogen bonded to the interlayer anions and water. The metal hydroxide sheets of an LDH with a Mg:Al ratio of 2:1 are shown with (B) random and (C) ordered cation distributions. Three major classes of hydroxyl groups are present in (B) (Mg₃-OH, Mg₂Al-OH, and MgAl₂-OH), whereas only one hydroxyl environment (Mg₂Al-OH) and one Mg local environment [Mg(OMg)₃(OAl)₃] are present in (C). [Reproduced with permission from American Association for the Advancement of Science (AAAS) of ref. 2]

2. Characterization and Synthesis

Local structure of the metal hydroxide layers

Understanding of the local structure of the metal hydroxide layers is of particular interest for the preparation of active catalysts. Recently, Sideris et al. elucidated the arrangement of divalent (Mg²⁺) and trivalent (Al³⁺) ions.² They unveiled that Mg²⁺ and Al³⁺ cations are not randomly distributed but completely ordered for a HT with Mg:Al ratio of 2:1 by using hydrogen nuclear magnetic resonance (¹H-NMR) spectroscopy under ultrafast magic angle spinning (MAS)

conditions. An extremely rapid MAS frequency (60 kHz) enables the individual H sites to be resolved whereas conventional MAS frequencies result broad featureless spectra. Each OH group in the layer is coordinated to three metals (each either Mg or Al), four hydroxyl local environments are possible; $\text{Mg}_3\text{-OH}$, $\text{Mg}_2\text{Al-OH}$, $\text{MgAl}_2\text{-OH}$, and $\text{Al}_3\text{-OH}$. Figure 1B and 1C show cation distributions of a HT with Mg:Al ratio of 2:1 with random and ordered fashions, respectively. In the case of random distribution model (Figure 1B), there are three hydroxyl environments, $\text{Mg}_2\text{-OH}$, $\text{Mg}_2\text{Al-OH}$, and $\text{MgAl}_2\text{-OH}$, and these distributions are calculated to be 30%, 44% and 22%, respectively. In contrast, ordered model (Figure 1C) has only one hydroxyl environment, $\text{Mg}_2\text{Al-OH}$ (99%). ^1H MAS NMR experiments revealed that a HT with Mg:Al ratio of 2:1 has mostly Mg_2AlOH (97%) and negligible Mg_3OH (3%), which is consistent with ordered model (Figure 1C). In addition, these results clearly indicate that there are no $\text{Al}^{3+}\text{-Al}^{3+}$ contacts in the hydroxide layers. For a HT with Mg:Al ratio of 3:1, distribution of hydroxyl groups of Mg_2AlOH and Mg_3OH is experimentally 20% and 80% respectively.

Sideris et al. also investigated Mg local environments by using high resolution multiple quantum (MQ) ^{25}Mg NMR spectroscopies to identify cation clustering in the metal hydroxide layers.⁸ The ordering of cations (Mg^{2+} and Al^{3+}) gradually increases with increasing Al content. Finally, a honeycomb-like Al distribution is formed for a Mg-Al HT with Mg:Al ratio of 2:1.

Thermal decomposition and subsequent rehydration of HT are usually carried out to obtain highly active solid base catalysts. Mg-Al- CO_3 HT dehydrates, dehydroxylates and decarbonates to form mixed metal oxide by calcination around 427 °C. The addition of water to the mixed oxide reconstructs the two-dimensional layer structure of Mg-Al compound. This interesting and unique behavior is called as “memory effect”. The reconstructed HT possesses OH^- anions which show very strong Brønsted basicity. Therefore, an investigation on local structure of mixed metal oxides is also of importance. Mourad et al. studied local structure of Mg-Al- CO_3 HT and corresponding mixed metal oxide by using in situ X-ray and neutron diffraction.⁹ X-ray diffraction reflects long-range structure, and neutron scattering is sensitive to the local atomic environment. Although much differences are found between HT and mixed metal oxide (calcined at 450 °C), the local structure of the cationic sheet is robust. Figure 2 shows pair distribution functions ($D(r)$) of HT at room temperature, 160 °C, 250 °C and mixed metal oxide (HT calcined at 450 °C), which are obtained from neutron scattering data. The main coordination environments and bond lengths of both the metal and oxygen atoms (M-O, M-M) for mixed metal oxide are very similar to those observed for the HT phases, indicating a subtle structure transformation mechanism. Although the periodic layer-layer structure collapses by calcination at 450 °C, the local cation environment remains unchanged. This is important information and can explain the origin of “memory effect”.

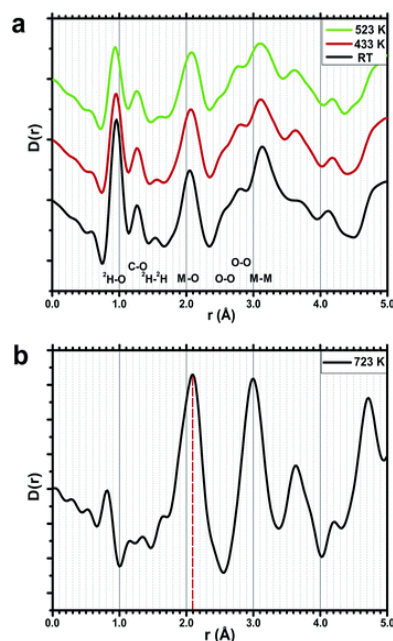


Figure 2 (A) Pair distribution functions (D(r)) of hydrotalcite at room temperature, 160 and 250 °C, obtained from neutron scattering data. The curves are plotted offset to increase the clarity of presentation. (B) Pair distribution function of mixed metal oxide at 450 °C. [Reproduced with permission from The Royal Society of Chemistry (RSC) of ref. 9]

Zhang et al. investigated the mechanism of the dehydration and dehydroxylation using thermogravimetry/differential thermal analysis/mass spectrometry (TG-DTA-MS).¹⁰ Figure 3 shows the TG-DTA-MS profiles of Mg-Al-CO₃ HT with Mg:Al ratio of 3:1. Water is released in four stages during thermal decomposition. Two-step dehydration and two-step dehydroxylation are observed. First, water molecules adsorbed on the surface and edge of HT are removed at low temperature region (194 °C). Then, water molecules intercalated within the layers desorb (256 °C). At a higher temperature, dehydroxylation of layer hydroxide groups occurs, resulting in the form of mixed metal oxide. After two-step dehydration, there are two MS ($m/z = 18$) peaks at 338 and 414 °C. According to ¹H MAS NMR by Sideris et al.,² there are 20% of Mg₃(OH) and 80% of Mg₂Al(OH) in the HT. From quantification of two peak areas, Zhang et al. have assigned MS peaks at 338 °C and 415 °C to dehydroxylation of Mg₃(OH) and Mg₂Al(OH), respectively. This result indicates Mg₂Al(OH) hydroxyl groups are thermally more stable than Mg₃(OH) hydroxyl groups.¹⁰

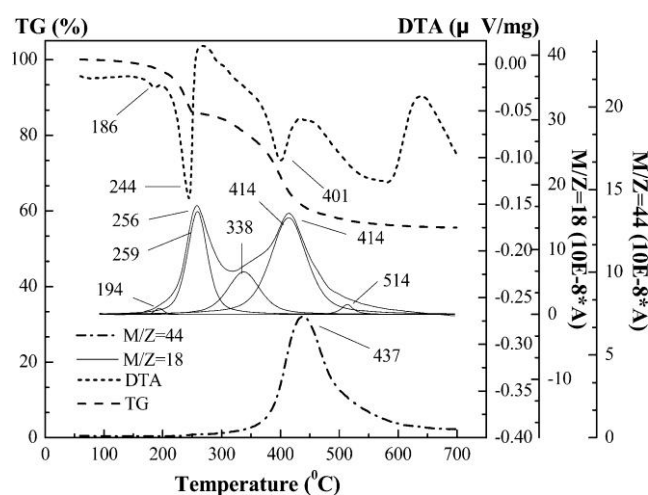


Figure 3 TG-DTA-MS curves of hydrotalcite ($\text{Mg}_3\text{Al-CO}_3$ HT). [Reproduced with permission from American Chemical Society (ACS) of ref. 10]

Catalytically active sites of HT are considered to be the edge of the crystallites because interlayer counterions are accessible to the bulk solution only at the edge. Roeffaers et al. revealed crystal-face-dependent catalysis of Li-Al layered double hydroxide (LDH) by in situ fluorescence microscopy.¹¹ By using 5-carboxyfluorescein diacetate as a fluorogenic reactant probe, direct observation of reactions (its ester hydrolysis and transesterification) was demonstrated. This method can verify real crystal-face active sites of LDH for such base-catalyzed reactions by single turnover counting. They found that hydrolysis of ester in water proceeds on the edge of the crystallite. On the contrary, transesterification with *n*-butanol, however, occurs on both the crystal surface and edges (less selectivity).

To elucidate the crystal-face-dependent catalysis of HT for transesterification and hydrolysis, Yu and Schmidt used a combination of molecular dynamics (MD) simulations and periodic plane-wave density functional theory (DFT).¹² They proposed that the catalytic activity can be explained by the adsorption free energies of the ester. Figure 4 shows representative illustration of the interaction of an ester, methyl butyrate with [001] surface and $[1\bar{1}0]$ surface. On the [001] surface, surface OH groups of HT perpendicularly interact with carbonyl oxygen C=O of the ester. Along the $[1\bar{1}0]$ interface, there is the formation of a strong Lewis acid-base adduct involving carbonyl oxygen C=O of the ester and interfacial coordinately unsaturated Mg^{2+} cations. Adsorption on the edge of the crystalline ($[1\bar{1}0]$ surface) is much more favorable as compared to the crystal surface ([001] surface). Therefore the edge of the crystalline is more active sites, which is consistent with hydrolysis results by Roeffaers et al.¹¹ On the other hand, less selectivity for transesterification can be explained by solvent effect. Adsorption free energies of ester are also influenced by solvents. Consequently, the reactivity on [001] surface in *n*-butanol (solvent for transesterification) would be greater than in water, resulting in less selectivity for transesterification.

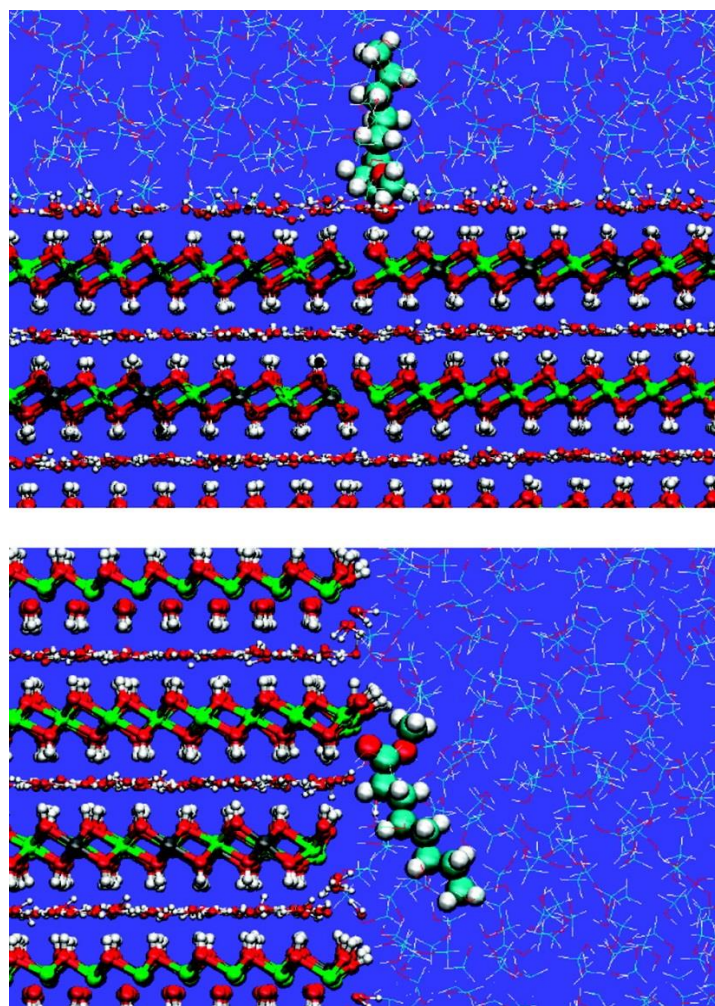


Figure 4 Representative illustration of the interaction of a model ester, methyl butyrate, with (top) [001] surface and (bottom) $[1 \bar{1} 0]$ surface. The HT is shown as balls-and-sticks, the methanol solvent as lines, and the ester as a space-filling model. Consistent with the periodic boundary conditions, a second HT interface occurs opposite the one shown here. [Reproduced with permission from American Chemical Society (ACS) of ref. 12]

Synthesis

Titration method, where homogeneously mixed solution of Mg^{2+} and Al^{3+} ions is precipitated by an alkali source such as sodium hydroxide and ammonia (or urea), has been widely applied for the preparation of HT. It is well known that a pH range between 7 and 10 is preferable for the synthesis of Mg-Al HT because the existence of aluminum precipitates (*ex.* $Al(OH)_3$ and $AlOOH$) and magnesium hydroxide ($Mg(OH)_2$) are obtained as an impurity at lower and higher pH values, respectively (Figure 5). Commonly, the pH value at 10 provides a well-crystallized and pure HT formation. Following the titration curves of $MgCl_2/AlCl_3$ solution during the pH rise with NaOH solution, Boclair and co-workers estimated the HT formation process as follows;^{13,14} the trivalent metal ions (Al^{3+}) are fully converted into aluminum hydroxide or hydrous oxide during increasing

the pH value of the mixed aqueous solution in the initial stage, thereafter, further addition of alkali (NaOH) precipitates the bivalent ions (Mg^{2+}) through the incorporation into aluminum hydrated oxide, then the Mg-Al HT is produced. In contrast, when the Mg/Al solution drops into the alkali solution, *i.e.* the pH of mother solution transforms from high to lower value, the formation process of Mg-Al HT is estimated as a direct conversion of $Al(OH)_4^-$ and $Mg(OH)_2$.^{15,16} It was considered that the impurity of $Mg(OH)_2$ is hardly formed in the presence of excess Al^{3+} ions even under a high pH value because the very stable state of $Al(OH)_4^-$ and ionic Mg^{2+} are immediately converted to the HT form.

The variable (turn-up or turn-down) pH method makes variation in the initial and end stages of HT precipitation process leading to inhomogeneous HT formation. Therefore, the attempt to keep pH value constant by alkali titration during addition of Mg/Al solution is examined. Figure 6(a) shows an example of morphology of HT prepared by the pH constant titration method. During the titration of the mixed aqueous solution (100 ml) of $Mg(NO_3)_2 \cdot 6H_2O$ (11.6 g) and $Al(NO_3)_3 \cdot 9H_2O$ (5.80 g) into $Na_2CO_3 \cdot 10H_2O$ (8.58 g) aqueous solution (120 ml) with a peristaltic pump at a speed of $0.6 \text{ ml} \cdot \text{min}^{-1}$, the pH was adjusted at 10 with a 1 M NaOH aqueous solution. The obtained suspension was aged at $60 \text{ }^\circ\text{C}$ for 2 h, then filtered, washed and dried at $100 \text{ }^\circ\text{C}$ overnight. Approximately 4.4 g HT (Mg/Al = 3) was obtained. The assemblies of whisker-like and thin plate-like nanoparticles were obtained, which is due to the initial crystal nuclei at the early crystallization stage of hexagonal HT. The XRD patterns also supported that the synthesized powder exhibited the HT structure and it had poor crystallinity estimated by a wide half-band widths. Thus, the simple titration method with mild aging likely fits for the synthesis of small HT particles. However, these basic titration methods have a limitation to control the nucleation and growth processes because 1) the drop of basic solution produces pH gradients during titration even under vigorous stirring, 2) the nuclei formed at the beginning of the titration are exposed to a much longer time for crystal growth process than those formed at the end of the titration, that serves a wide size distribution of crystallite and particle sizes.

To control the nucleation, crystal-growth and aggregation processes during HT formation, Zhao et al. released the immediate nucleation process using a colloid mill rotating at 3000 rpm.¹⁷ Abello and Perez-Ramirez investigated an in-line dispersion-precipitation (ILDLP) method using a home-made microreactor.¹⁸ The ILDP method is that aqueous solutions of $Mg(NO_3)_2$, $Al(NO_3)_3$ and $NaOH/Na_2CO_3$ are continuously fed at room temperature into precipitation chamber with stirring at very high speed (6,500-24,000 rpm), then the Mg-Al HT slurry is obtained. The average crystallite size and the porosity of HT are predictable by changing the residence time and/or stirring speeds in the chamber.

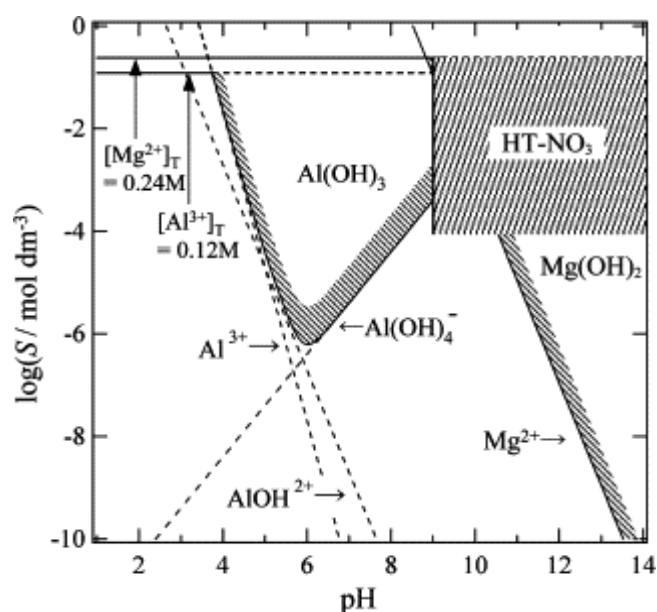


Figure 5 Domain diagram of Al(OH)₃, Mg(OH)₂, and Mg-Al-NO₃ hydroxalcite. [Reproduced with permission from Elsevier of ref. 19] Note that the solubility denoted as “S” in the axis.

Conventionally, the homogeneous nucleation and growth of LDHs are accommodated by using hydrolysis of urea which releases ammonia and carbonate ions into the solution and achieves gradual and uniform increase of pH in the solution.^{20,21} Figure 6(b) shows an example of the as-synthesized HT morphology by urea method. The mixtures of Mg(NO₃)₂•6H₂O (9.7 g) and Al(NO₃)₃•9H₂O (4.8 g) in deionized water (1000 ml) were precipitated by the urea (30 g) hydrolysis method at 92 °C for 24 h with vigorous stirring. The obtained suspension was filtered, washed and dried at 100 °C overnight. Approximately 2.6 g HT (Mg/Al = 3) was obtained. As shown in the Figure 6(b), well-crystallized and typical hexagonal-structured HTs were obtained by the urea method. The XRD patterns also supported that the synthesized powder exhibited the HT structure with good crystallinity. The nucleation and growth process can be controlled by the urea concentration and hydrolysis temperature. However, a disadvantage of the urea hydrolysis method is that the slow hydrolysis of urea leads slow nucleation and a low degree of supersaturation during precipitation resulting in the large size HT particles.²²

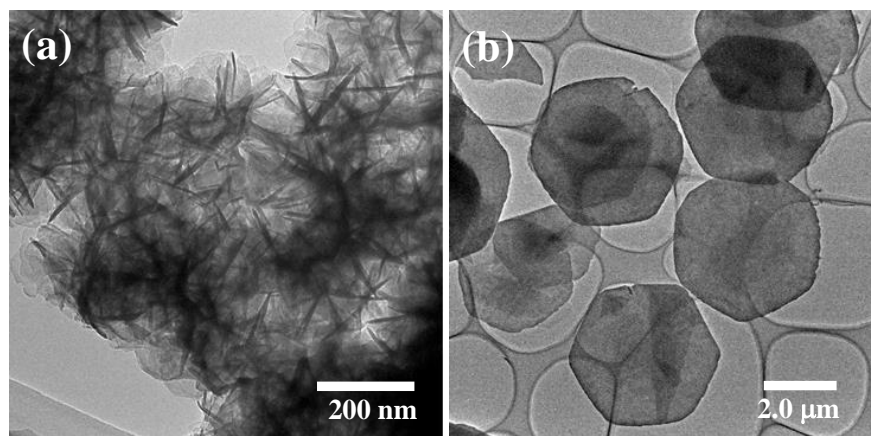


Figure 6 TEM images of the as-synthesized hydrotalcite (Mg/Al = 3) by (a) co-precipitation and (b) urea hydrolysis method.

Zhang et al. proposed a detailed formation mechanism of Mg-Al HT with careful investigations using $\text{Mg}(\text{NO}_3)_2$ and $\text{Al}(\text{NO}_3)_3$ by urea precipitation method as shown in Figure 7.²³ The first stage corresponds to the formation of amorphous aluminum hydroxide in the presence of excess Al^{3+} ions (step 1). Simultaneously, an in situ phase transformation from amorphous aluminum to lamellar boehmite occurs, forming alveolate-like agglomerates of boehmite particles (step 2). In this stage, anionic ions (NO_3^-) and Mg^{2+} are adsorbed onto the surface. Thereafter, the surface-adsorbed Mg^{2+} ions substitute Al^{3+} of the AlO_6 octahedra in the crystallites of oxide-hydroxide aluminum boehmite $\gamma\text{-AlOOH}$, it leads the charge imbalance of the sheets and destruction of the interlamellar hydrogen bonds in boehmite lamellar, then, the intercalation of CO_3^{2-} into the interlayer begins for balancing the charges between sheets (step 3). Subsequently, the crystallization and growth of HT crystallites occur from the exterior to the interior of the aggregates (step 4). Finally, the integrated HT hexagonal plates are formed (step 5). These proposed mechanisms agree well with previous observations in the co-precipitation method (*vide supra*). Following these reports, the combined use of the co-precipitation and urea hydrolysis methods for nucleation and growth controls, respectively, seems to be one of the effective approaches of the fine HT particles synthesis.

Notably, to obtain uniform HTs, a combination of a faster nucleation by NaOH and a uniform growth in hydrothermal condition was attempted by Xu et al.²⁴ The large hexagonal plate HT was produced by a continuous crystal growth of the nuclei precipitated by NaOH following the Ostwald ripening process with aging treatment under high temperature. The synthesized HT possessed controllable particle sizes in 50-300 nm with the aspect ratio about 5-10 by changing temperature and time. Interestingly, Wang et al. focused the important relationship between the synthesis pH and the isoelectric point (IEP) of HTs during the HT synthesis with co-precipitation of $\text{Al}(\text{NO}_3)_3$ and $\text{Mg}(\text{NO}_3)_2$ at constant pH follows to the hydrothermal treatment.²⁵ They observed that the “rosette”

types of HT particles were formed at pH 10 whereas the Mg-Al HT nanoparticle aggregates were produced at pH 11-14. Note that the IEP of HT is around 10. In the pH = 10 condition, the formation of the primary particles is fast but the growth is slow because the surface of HT is electrically neutral. Consequently, the HT crystal growth is preferred along the (001) plane, resulting in the “rosette” HT. The (001) plane has the lowest surface charge density and thus it is stable under the synthesis condition. On the other hand, in the pH = 11-14 condition, the surface of HT was more negatively charged resulting in the precipitation of $Mg(OH)_2$ and its conversion to HT became faster while the interaction between HT and anionic ions represented as $Al(OH)_4^-$, NO_3^- , CO_3^{2-} and/or OH^- was strongly prohibited. Thus, the HT nanoparticle aggregates were produced. Briefly, the aspect ratio of HT plates decreased with increase of alkali concentration. These results support that the alkali concentration affects not only nucleation but also growth processes in the HT formation.

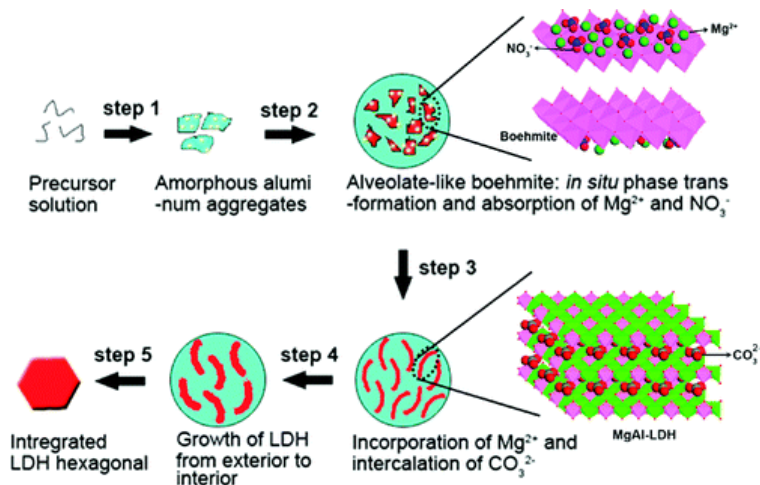


Figure 7 Schematic illustration of a proposed crystal evolution process of Mg-Al hydroxalite. [Reproduced with permission from American Chemical Society (ACS) of ref. 23]

As mentioned above, the active sites for base-catalyzed reactions are mainly attributed to the edge of the crystallite. This motivates researchers to synthesize HT particles with very small sizes. Fabrication of such nano-sized HT has been achieved by confinement within restricted spaces. Winter et al. synthesized HT platelets in the pore of carbon nanofibers (HT/CNF) (Figure 8).²⁶ Li et al. fabricated HT platelets within silica mesopores (SBA-HT).²⁷ The lateral sizes of HT are 20 nm and less than 9 nm for HT/CNF and SBA-HT, respectively, much smaller than 60-70 nm which is typical sizes prepared by conventional precipitation method. These HT nanocrystallites possess a large amount of base sites. Amounts of CO_2 adsorption are $0.75 \text{ mmol}\cdot\text{g}^{-1}$ and $1.21 \text{ mmol}\cdot\text{g}^{-1}$ for HT/CNF and SBA-HT, respectively, resulting in the high catalytic activity for base-catalyzed reaction, aldol condensation of acetone at 0°C .

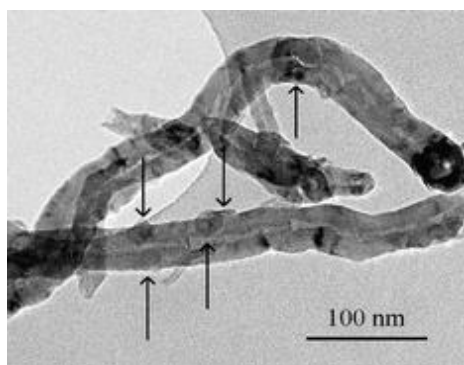


Figure 8 TEM image of hydrotalcite/carbon nanofiber (HT/CNF). [Reproduced with permission from The Royal Society of Chemistry (RCS) of ref. 26]

In some cases, mass-transport limitation should be considered particularly for reactions using bulky reactants. Geraud et al. synthesized the 3D macroscopically ordered HT prepared by a co-precipitation method with polystyrene (820 nm sphere type) template.²⁸ They obtained a high surface area ($202 \text{ m}^2 \cdot \text{g}^{-1}$) derived from their dual (macro- and meso-) porosities after calcination treatment at $400 \text{ }^\circ\text{C}$. With intercalation of decatungstate anion ($\text{W}_{10}\text{O}_{32}^-$) into an open macroporous framework of the HT structure, a good photocatalytic performance for the photodegradation of 2,6-dimethylphenol was observed because the accessibility of UV-light to intercalated decatungstate and the reactant diffusion were drastically increased in the ordered macroporous HT.²⁹ Biodiesel production using porous HT is one of typical examples for consideration of mass-transport limitation because the reaction is transesterification of long-chain triglycerides with methanol. Woodford et al. synthesized macroporous Mg-Al hydrotalcite (MacroHT) catalyst by using monodispersed polystyrene bead (*ca.* 350 nm) as template (Figure 9).³⁰ Owing to the presence of macropores, the MacroHT exhibited much higher turnover frequencies (TOFs) for transesterification of long-chain triglycerides (C12 and C18) than conventional HT.

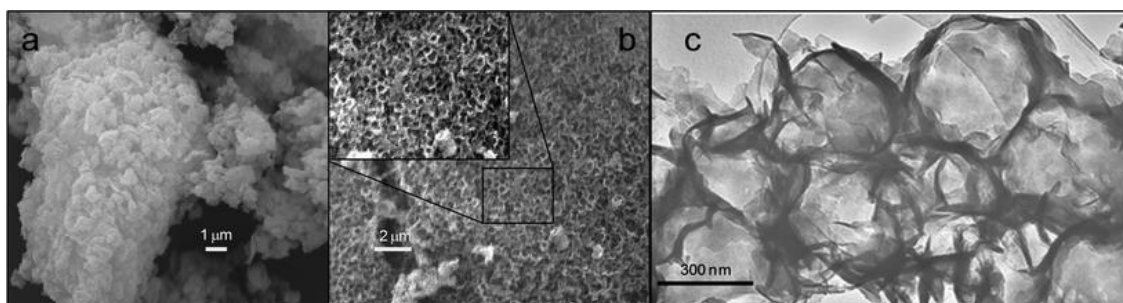


Figure 9 SEM images of (a) conventional hydrotalcite and (b) macroporous hydrotalcite, and (c) TEM image of macroporous hydrotalcite highlighting macropores and thin hydrotalcite walls. [Reproduced with permission from The Royal Society of Chemistry (RCS) of ref. 30]

As advanced HTs, two-dimensional LDH nanosheet materials have been widely investigated in recent years because they exhibited unusual physical properties such as a quantum size effect associated to their ultra-thin structure and became building blocks for unique hybrid materials.³¹ Because carbonate ion, the most typical HT builder, has exceptionally high affinity to HTs comparing with other anions, deintercalation of carbonate in HTs with another anions is required before delamination process; the preference of HTs for different anions is reported in the order of $\text{CO}_3^{2-} > \text{SO}_4^{2-} > \text{OH}^- > \text{F}^- > \text{Cl}^- > \text{Br}^- > \text{NO}_3^- > \text{I}^-$.³² In order to displace carbonate ions into other anions (typically, nitrate or chloride ions) without damaging the HT host plate, decarbonation treatment using a large excess of salts and a much diluted acid was found to be an effective process.³³ After decarbonation, the reaction of formamide on the HT leads to exfoliation of the HT host plates under soaking for a few days with stirring.³⁴ Under ultrasonic treatment, the penetration of formamide was accelerated, leading earlier exfoliation. Delamination mechanism of LDH by formamide was described as two-stages; rapid swelling and subsequent slow exfoliation.³⁵ In general, these delamination processes are applied to the well-crystallized and micron-sized LDH platelets (typically hexagonal shape) prepared by a hydrothermal process and/or urea method, to afford submicron-sized HT nanosheets. Nano-sized HT nanosheets are feasible by delamination of submicron-sized HT crystallites prepared with a conventional co-precipitation method, however their stabilities and applications seem to be limited. The exfoliated HT has been applied for the synthesis of advanced materials such as a magnetic HT nanocomposite,³⁶ a hollow nanoshell of HT³⁷ and an ultrathin HT film.³⁸

Microwave irradiation treatment (MWIT) has been employed to accelerate the rate of nucleation and growth of HT crystals.^{39,40} MWIT affects the textual properties of HTs such as specific surface area, narrow particle size distribution, improved thermal stability and well-ordered crystal structure. The effect of MWIT is dependent on various factors including the nature of cations and anions in the HTs, metal ratios (Mg/Al), the synthesis method and the activation conditions.^{41,42} In some cases, increase of porosity has been observed by MWIT, which is related to be a loss of aluminum from the layer structure (dealumination) due to the local overheating.⁴³

MWIT also affects the acid-base properties of HTs. Tichit et al. focused on not only structural but also acid-base properties of the HTs obtained by MWIT.⁴⁴ MWIT was used for co-precipitated gel followed by calcination. Interestingly, the adsorption microcalorimetry using CO_2 and FTIR spectroscopy using CH_3CN indicated that the Mg-Al mixed oxides obtained by calcination of the HT with MWIT showed higher amounts of acidic and basic sites than that without MWIT. They concluded that the MWIT probably induces higher amounts of surface defect sites. It was also reported that MWIT during HT synthesis through both co-precipitation step and aging step resulted in increase of the amount of defect sites in the calcined HTs (i.e. Mg-Al mixed oxides).⁴⁵ In addition,

MWIT was effective for synthesis of HTs with unique morphology such as onion-like⁴⁶ and donut-shaped⁴⁷ structures.

Magnetic HT has attracted attention in this decade because it can be used as reservoirs for drugs and biomolecules⁴⁸ and magnetically separable base catalysts or supports. The HT synthesis by co-precipitation method in the presence of magnetic particles such as CoFe_2O_4 and MgFe_2O_4 spinels was proposed as a one process for preparing the magnetic HTs.^{49,50} By using the monodispersed magnetic Fe_3O_4 nanoparticles (*ca.* 20 nm) as nanomagnets, Nishimura et al. synthesized magnetically separable HT catalysts which have good property for easy handling.⁵¹ The magnetizations of the prepared magnetic HTs were controlled in the range of between 0.20 and 2.0 $\text{emu}\cdot\text{g}^{-1}$ measured at 300 K by changing the concentration of Fe (0.28-2.99 wt%). Notably, the synthesis of a core-shell type of magnetic HT composite has been announced by some groups in recent years. By the selective deposition and formation of HT onto the Fe_3O_4 submicro-spheres (220 or 450 nm) surface, Zhang and co-workers obtained the monodispersed and well-coated $\text{Fe}_3\text{O}_4@\text{HT}$ and $\text{Au}/(\text{Fe}_3\text{O}_4@\text{HT})$ particles with diameters of 250-260 nm and 100-200 nm, respectively.^{52,53} They also attempted to adsorb the anticancer agent doxifluridine (DFUR) as a model drug onto the $\text{Fe}_3\text{O}_4@\text{HT}$. These demonstrations indicated that the core-shell magnetic HTs were capable for both reservoir of the anticancer agent and support for metal catalyst. Some of the authors also reported the $(\text{Fe}_3\text{O}_4@\text{SiO}_2)@\text{Ni-Al}$ HT microspheres *via* the precipitation of $\text{Ni}(\text{NO}_3)_2$ solution into the $(\text{Fe}_3\text{O}_4@\text{SiO}_2)@\text{AlOOH}$ microsphere.⁵⁴ This achievement supported the proposed formation mechanism of HT-like materials *via* AlOOH phase as mentioned above. On the other hand, Liang et al. fabricated fine core-shell type of magnetic HT nanocomposite, silica-coated Fe_3O_4 (*ca.* 400 nm) encapsulated Mg-Al HT nanosheets, using the HT nanosheet as the shell construction agent.³⁶ These achievements inspired us to attempt the creation of another types of magnetic HT composite with combinations of the Fe_3O_4 nanomagnet (*ca.* 20 nm)⁵¹ and the exfoliation tendency of HT in formamide solution.^{33,34} Firstly, HTs possessing a large flat plane were prepared by urea method. The mixtures of $\text{Mg}(\text{NO}_3)_2\cdot 6\text{H}_2\text{O}$ (5.4 g) and $\text{Al}(\text{NO}_3)_3\cdot 9\text{H}_2\text{O}$ (1.6 g) in deionized water (1000 ml) were stirred with urea (15 g) at 92 °C for 24 h. The obtained suspension was filtered, washed and dried at 100 °C overnight. Approximately 0.85 g HT (Mg/Al = 5) was obtained. Interestingly, the synthesized HT exhibited the circle-like morphology as shown in Figure 10(a). It was found that the alkali concentration leads to size increase from nanosheets, nanoparticles to disk-like crystals; *i.e.* alkali concentration changes the aspect ratio of HT,^{55,56} which implies that the alkali affects not only nucleation but also growth and aggregation processes. Though the detailed formation mechanism remains unclear, we supposed that the low concentration of urea prevented the growth of HT nuclei to the hexagonal structure, resulting in the circle-like morphology as shown in Figure 10(a). As-prepared HT (0.6 g) and formamide (50 ml) were stirred for 3 h, then the dispersion of tetramethylammonium hydroxide (TMAOH) capped Fe_3O_4 nanoparticles (10 ml)⁵¹ was added and

further stirred for 3 days at room temperature. The obtained suspension was aged at 333 K for 2.5 h in the presence of a 1 M NaOH/Na₂CO₃ (= 2/1) aqueous solution (10 ml), then filtered, washed and dried at 100 °C overnight. Figure 10(b) shows TEM images of the as-synthesized nanosheet-like magnetic HT. It was confirmed that there were highly dispersed Fe₃O₄ nanoparticles on the sheet-like HT surface (Figure 10(c)). The synthesized nanosheet-like magnetic HT was easily separated from solution by a magnetic field (NdFeB magnet of ca. 460 mT).⁵⁷

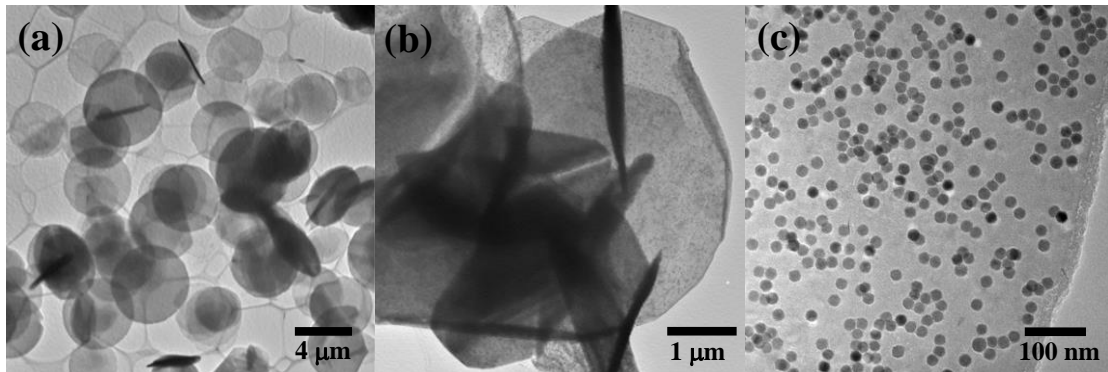


Figure 10 TEM images of the as-synthesized hydrotalcite (Mg/Al = 5), (a) after urea synthesis and (b,c) after adsorption of Fe₃O₄ nanomagnets in different magnifications.

Creation of the large-scale uniform HT films has been gradually attracted in the area of sensor and electrode materials. Basically, preparations of film type of HTs were attempted by Langmuir-Blodgett deposition method (LB method)^{58,59} and spin coat technology.⁶⁰ Synthesis of HT films onto the substrate under hydrothermal condition is one of the effective approaches for controlling the orientation of the HT film. Chen et al. obtained the oriented HT film under hydrothermal condition.⁵⁵ Direct synthesis on porous anodic alumina/aluminum substrate following a growth process under a hydrothermal treatment was proposed by Duan et al. for HTs such as Ni-Al HT and Zn-Al HT.^{61,62} These processes allowed the control of thickness and pore size or wetting properties of HT-like films. To build the layer-by-layer assembly and selective layer expansion, Lee et al. used the carboxyalkylphosphonic acids as a graft agent between HT prepared by co-precipitation and hydrothermal treatment method and the surface of Si substrates.⁶³ The authors also created a new polymer-HT hybrid film using a surface selective deposition of poly(methyl methacrylate) (PMMA) by UV-induced polymerization without using any additional linker.⁶⁴ The PMMA/HT hybrid film showed an excellent UV blocking effect for wavelength below 350 nm. Duan et al. created ultrathin films by stacking exfoliated HT monolayers with π -conjugated polymers, *ex.* a sulfonated poly(*p*-phenylene). The fabricated inorganic/organic hybrid HT films had a long fluorescence lifetime and a high photostability for UV irradiation.^{38,65}

As mentioned above, synthesis processes and applications of HT materials are favored in many advanced areas. The HT-like materials still have a lot of possibilities to open up new platform of

other chemical interfaces. Some of recent interesting achievements are introduced in the following sections.

3. Base-catalyzed Reactions by Hydrotalcites

The HT is a unique solid which can be stored in air atmosphere and exhibits basic character without any pretreatment. The base sites of the HT are originated from HCO_3^- species on the hydrophilic HT surface. The anions in the interlayer space cannot participate in the reaction because of the limited space of the HT interlayer. The surface basic property can be tuned by varying Mg/Al ratio or anionic species in the interlayer space.³ For example, exchange the NO_3^- ions into O-*t*-Bu anion produced an efficient base catalyst for aldol condensation of aldehydes with acetone.⁶⁶ Hydrophilic nature of the basic HT catalyst enables the epoxidation of α,β -unsaturated ketones using H_2O_2 as a oxidizing reagent without organic solvent.⁶⁷ The importance of basicity of HT has been reported for the epoxidation of olefins using H_2O_2 and amide compounds^{68,69} as well as the Baeyer-Villiger oxidation.⁷⁰ The catalysis of HTs for C-C bond formation such as aldol condensation and oxidation including Baeyer-Villiger reaction has been reviewed.⁷ This part focuses on recent literatures for base catalysis of the HT materials, especially for transesterification, isomerization of glucose and the Knoevenagel condensation.

Transesterification of vegetable oils or animal fats with methanol is the conventional method for biodiesel fuel (BDF) production and which can be facilitated by both Brønsted acid and base catalysts. Transesterification of triglyceride with methanol over the Mg-rich uncalcined HT⁷¹ and reconstructed HT^{72,73} indicated good activities owing to their high basicities. Ca-containing solid base catalysts such as KF/Ca-Mg-Al HT and Ca/Al or Ca/Mg mixed oxide produced via calcination of LDHs were also applied for the transesterification of vegetable oil and methanol,⁷⁴⁻⁷⁷ however, it is afraid that calcium diglyceroxides could be formed by the interaction between Ca^{2+} ion and glycerol, which will be main soluble species.⁷⁸⁻⁸⁰ Meyer et al. investigated the influence of interlayer anion in HT precursors on the catalytic activity for transesterification over mixed oxides derived from HT by calcination at 450 °C.⁸¹ By comparing with various aliphatic terminal dicarboxylate interlayer anions, it was confirmed that the pore size distributions of the derived mixed oxide were influenced by the nature of the interlayer anions in HT, and the higher activity of mixed oxides was attributed mainly to wider pores, enabling better accessibility for bulky triglyceride molecules. Recently, it was reported that uncalcined macroporous HT also achieved improvement of the diffusion of bulky triglycerides and accessibility of active sites within the hierarchical macropore-micropore architecture.³⁰ Consequently, not only the amount of basicity but also the accessibility were important factors for transesterification over HT derived catalysts.

Chemical reactions for utilization of huge amount of glycerol originated from BDF synthesis have been investigated. Synthesis of cyclic carbonate by the base catalyzed proton elimination from glycerol is one of the key reactions. Glycerol-derived glycerol carbonate (GC) is widely used as

protic solvent and intermediate of polycarbonates and polyesters. Takagaki et al. reported that uncalcined HT involving hydromagnesite (HM), $\text{Mg}_5(\text{CO}_3)_4(\text{OH})_2 \cdot 4\text{H}_2\text{O}$, showed a significant activity for the transesterifications of glycols with dialkyl carbonate affording to GC in a batch reactor with and without organic solvent.⁸² The synthesized HT-HM catalyst is reusable for above 3rd runs. They proposed that the coexistence of HM enhanced the catalytic activity of the HT since it increased both surface area and the number of adsorption sites of substrates on the catalyst surface.⁸³ For modifying the type of basic centre on the HT, Alvarez et al. performed a rehydration of the calcined HT catalyst applying the memory effect origin and obtained an active catalyst for transesterification of glycerol in a batch and flow reactors.⁸⁴⁻⁸⁶ Urea and ethylene carbonate (EC) are also investigated carbon source for GC synthesis from glycerol. Climent et al. reported that the well-balanced acid-base catalyst, Al/Zn mixed oxide prepared by calcination of Al-Zn HT-like compounds, produced an enhancement of the synthesis of GC in the presence of urea.⁸⁷ They also found that HT and Li-substituted HT, $[\text{Al}_2\text{Li}(\text{OH})_6]_2\text{CO}_3 \cdot m\text{H}_2\text{O}$, catalysts gave a high yield of GC with a high selectivity from the reaction of EC with glycerol. These catalysts kept good activities in 3rd cycle in DMF solvent. For the synthesis of glycerol carbonate, increasing the base strength induces a high conversion of glycerol with a very low selectivity for GC. Therefore, it is important to control the number of base sites to enhance the catalysis by co-existent acid site.

Isomerization of glucose, obtained by the depolymerization of cellulose, into fructose is a key reaction to utilize inedible biomass-derived compounds. Solid Lewis acid catalyst is known to promote this isomerization.⁸⁸ The Mg-Al HT was also found to show a high activity for the skeletal isomerization of glucose to fructose in water⁸⁹ or DMF solvent.^{90,91} The above unique base catalysis of the HT materials for the sugar isomerization could be further applied for the one-pot synthesis combined with solid acid catalyst (*vide infra*).

The memory effect of the HT has been already introduced in Part 2 in this review. This memory effect is utilized for an exchange of CO_3^{2-} (in the interlayer) and HCO_3^- species (on the surface) with OH^- anions. After calcination of the HT under Ar flow at 450 °C, hydration was performed at room temperature under an Ar flow in water to reconstruct the original layered structure (reconstructed HT). The reconstructed HT possesses base sites associated with OH^- anions and shows excellent catalytic activity for the Knoevenagel condensation of various aldehydes with nitriles in the presence of water as well as aqueous Michael reaction of nitriles with α,β -unsaturated compounds.⁹² It should be noted that the original HT with CO_3^{2-} and HCO_3^- species did not show any catalytic activity for the above reactions.⁹³

As a further example of organic reaction catalyzed by HT, Lemos and Lourenço reported syntheses of dihydro-1,2-oxazines, tetrahydropyridazines, and isoxazolines by [4+2] and [3+2] cycloadditions of heterocycles with olefins using HT in the absence of organic solvent.⁹⁴

4. Hydrotalcite as Support for Metal Catalysts

When immobilized metal species on solid supports are used as catalysts in liquid-phase, a possibility of leaching of active metal species into the solution is always apprehended. Leaching of active metal species and stability of active species can be checked by confirming the reusability of the catalyst, reaction progress after hot-filtration of the catalyst, and ICP analysis of metal species in the reaction mixture after a catalyst removal. Stability of the oxidation states, morphology, particle size of active metal species can be evaluated by XAFS, TEM, and XRD analyses of used catalyst (*vide infra*).

As mentioned in the previous section, various metal species can be immobilized either on the surface of the HT (adsorption ability), or in the Brucite layer (cation exchange ability) or within the interlayer space (anion exchange ability) to form HT-supported metal catalysts (Figure 11). Type (a) catalyst can be prepared by immobilization using metal salts (or metal clusters) solution with HT *via* adsorption. Type (b) catalyst can be obtained by addition of metal compounds to Mg^{2+} and Al^{3+} -containing solution during synthesis of HT. Together with Mg^{2+} and Al^{3+} , metal cations are incorporated in the Brucite layer. Type (c) catalyst can be made by anion-exchange reaction of metal anions with anions within the interlayer spaces such as carbonates.

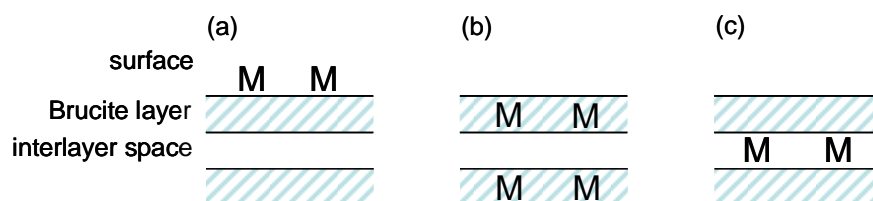
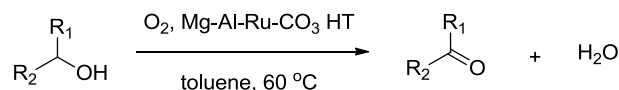


Figure 11 Immobilization of metal species (M) on the surface (a), in the Brucite layer (b) and within the interlayer space (c) of the hydrotalcite.

The most important character of the HT as metal support is its surface basicity which promotes the abstraction of protons from organic molecules especially from alcohols even after metal immobilization. This abstraction step is considered as the initial step for the dehydrogenation of alcohols to form metal-alcoholate intermediates, which undergoes β -hydride elimination to afford the corresponding carbonyl compounds. This section is divided into subsections according to the metal element and mainly focuses on the dehydrogenative oxidation of alcohols and deoxygenation of epoxides mediated by metal species on the HT. The regulation of an interaction between metal species using the HT crystals is also introduced.

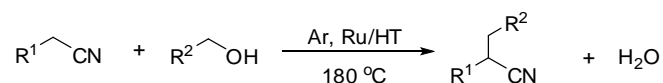
Ruthenium

The Mg and Al cations in the Brucite layer can be replaced by ruthenium cations to form the Mg-Al-Ru-CO₃ HT catalyst for the oxidation of allylic and benzylic alcohols into the corresponding carbonyl compounds at 60 °C in toluene solvent (Scheme 1).⁹⁵



Scheme 1 Oxidative dehydrogenation of alcohols using molecular oxygen

The alcohol oxidation proceeds *via* proton abstraction of alcohol to form Ru-alcoholate intermediates, which undergo β-hydride elimination to afford the carbonyl compound and Ru-H species. The oxidation of the Ru-H species by molecular oxygen and subsequent ligand exchange with another alcohol completes the catalytic cycle. Therefore, when the reaction of alcohol is performed in the absence of oxygen, the carbonyl compound is formed and the Ru-H species remains. It was found that the Ru-H species are able to hydrogenate olefinic bond as follows. When the primary alcohols were reacted with nitriles in the absence of oxygen using the hydrotalcite-grafted Ru species (Ru/HT), α-alkylated nitriles were formed (Scheme 2).^{96,97} First, the primary alcohols are oxidized into the aldehydes to afford the Ru-H species. The surface base sites of the HT catalyze the aldol condensation of nitriles with aldehydes to afford α,β-unsaturated nitriles, followed by the hydrogenation with the Ru-H species to give α-alkylated nitriles. The primary alcohols also acted as a solvent. The reaction in the presence of oxygen did not give the α-alkylated nitriles.



Scheme 2 α-Alkylation of nitriles with primary alcohols

As discussed later, the efficiency of the Ru cation species on the HT surface is higher than that of those in the Brucite layer. The fine structure of the Ru species on the HT was analyzed by Ru K-edge X-ray-absorption fine-structure spectroscopy (XAFS) technique. The X-ray absorption near-edge structure (XANES) spectrum of the Ru/HT was similar to that of Ru^{IV}O₂ but differed from that of Ru^{III}(acac)₃, implying that the Ru species is in the +4 oxidation state. The extended X-ray absorption fine structure (EXAFS) analysis suggested a monomeric Ru(IV) species having one hydroxyl and two water ligands grafted on a triad of oxygen atoms on the HT surface.^{96,97}

The catalytic feature of the Ru species associated with the HT in the alcohol oxidation is high selectivity toward aldehyde. The Ru/HT scarcely catalyzes the aldehyde oxidation into the

corresponding carboxylic acids. Furthermore, the Ru/HT does not show the catalytic activity in water solvent. The Ru/HT has been applied to the selective oxidation of 5-hydroxymethylfurfural (HMF) into 2,5-diformylfuran (DFF) selectively in *N,N*-dimethylformamide (DMF) solvent (*vide infra*)⁹⁸ and selective hydrogenation of aldohexoses into sugar alcohols in the presence of both H₂ and isopropanol in water.⁹⁹

The methodology for functionalization of the Ru species by other metals will be introduced later.

Palladium

The HT-grafted Pd(II) species (Pd/HT) efficiently catalyzes the aerobic oxidation in toluene solvent of primary and secondary alcohols into the corresponding carbonyl compounds with the aid of pyridine at 60 °C.¹⁰⁰ Allylic alcohols were also oxidized without any isomerization of an olefinic part. The HT-grafted Pd nanoparticles (Pd_{nano}/HT), with a mean diameter of *ca.* 7 nm, promote consecutive aldol reaction/hydrogenation to afford α -alkylated nitriles from nitriles and aldehydes in toluene solvent.¹⁰¹ The basic sites of the HT promote aldol reaction of nitriles with aldehydes to afford unsaturated nitriles, followed by the Pd-catalyzed hydrogenation to give α -alkylated nitriles in the presence of H₂.

Silver

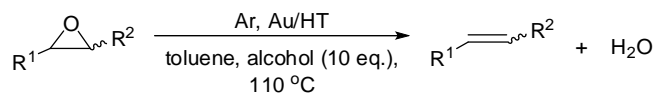
Ag nanoparticles with 3.3 nm mean diameter immobilized on the HT surface (Ag_{nano}/HT) efficiently catalyze the dehydrogenation of alcohols under oxygen-free conditions at 130 °C to afford the corresponding carbonyl compounds with coproduction of equivalent molar amounts of H₂ in *p*-xylene solvent.¹⁰² High chemoselectivity of the Ag_{nano}/HT catalyst toward dehydrogenation was compared in the reaction of cinnamyl alcohol under Ar atmosphere with Ru/HT and Pd_{nano}/HT catalysts. For the Ru/HT and Pd_{nano}/HT catalysts, the hydrogen transfer and isomerization occurred, whereas the Ag_{nano}/HT catalyst exclusively gave cinnamaldehyde.

Gold

Recently, much attention has been paid to the development of Au nanoparticle catalysts due to their size-dependent behaviors.^{103,104} The HT-grafted Au nanoparticles (Au_{nano}/HT) with a mean diameter of 2.7 nm are found to be reusable as heterogeneous catalysts for synthesis of lactones from diols using molecular oxygen as an oxidant with a high turnover number (TON) of 1,400 in toluene solvent.¹⁰⁵ The Au nanoparticles are generally prepared by deposition of Au chloride in water, followed by the addition of NH₃ (aq.) and by reduction using KBH₄.

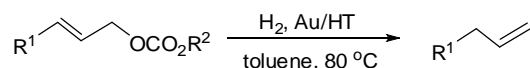
The Au_{nano}/HT also catalyzes the deoxygenation of epoxides into the corresponding olefins under Ar atmosphere in the presence of 10 equiv. of 2-propanol in toluene solvent (Scheme 3).¹⁰⁶ The Au nanoparticles and basic sites of the HT surface cooperatively work for the above deoxygenation of

the epoxides. The proton species on the HT surface (from the alcohol) opens the epoxide, and subsequent attack of the Au-H species and dehydration of the surface intermediates provides the olefins.



Scheme 3 Deoxygenation of epoxides

Deoxygenation of epoxides into olefins is also possible using Au_{nano}/HT catalysts under H₂ atmosphere in toluene solvent.¹⁰⁷ High selectivity toward olefins can be rationalized by the lack of olefin hydrogenation ability of the Au_{nano}/HT catalyst even in the presence of H₂. It was also shown that the epoxide deoxygenation is dependent on the size of the Au particles. Small Au nanoparticles of less than 3 nm are essential for the deoxygenation. The concerted effect of Au nanoparticles and basic sites of the HT surface has been proposed. The cooperative action between Au nanoparticles and base sites of the HT surface is also suggested to promote chemoselective hydrogenolysis of allylic carbonates to the terminal olefins using an H₂ as a reductant in toluene solvent (Scheme 4).¹⁰⁸ The isotope experiment using D₂ instead of H₂ suggests that the Au_{nano}/HT-catalyzed hydrogenolysis may mainly proceed *via* π-allyl intermediate generated from an allylic carbonate.

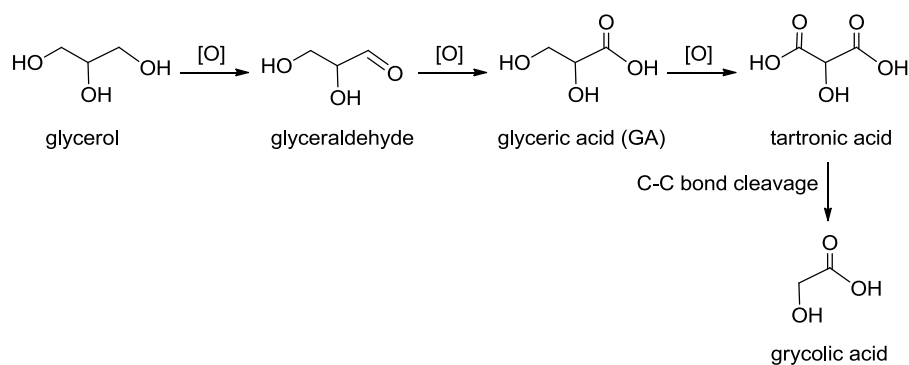


Scheme 4 Chemoselective hydrogenolysis of allylic carbonates

The Au nanoparticles on the HT surface also promote the oxidant-free dehydrogenation of alcohols in *p*-xylene solvent.¹⁰⁹ It was shown that the catalytic activity of the Au_{nano}/HT strongly depends on Au content, the small Au particles are more active than large particles. The HT-supported Au-nanoparticle (3.2 nm in average size) catalyze highly efficient base-free oxidation of 5-hydroxymethylfurfural (HMF) into 2,5-furandicarboxylic acid (FDCA) under atmospheric oxygen pressure in water solvent.¹¹⁰ The Au_{nano}/HT catalyst could be reused at least three times without significant loss of activity. Stability of Au oxidation state, morphology, and particle size was evidenced by XAFS and TEM measurements of the sample after the reaction. After the catalyst removal, no change of product yield was observed. Furthermore, ICP analysis of the filtrate solution gave no gold species. These results indicate that gold species were stable during the reaction and were not leached from the HT support.

Importance of the calcination temperature for the synthesis of Au⁰ species on the HT surface was

investigated for glycerol oxidation. The Au^{3+} precursor expected as a $\{[\text{Au}(\text{NH}_3)_2(\text{H}_2\text{O})_{2-x}(\text{OH})_x]^{(3-x)}\}^+$ cationic complex showed a gradual reduction to Au metal by increasing the calcination temperature because it was a thermodynamically favorable reaction. The Au^0 nanoparticle in the $\text{Au}_{\text{nano}}/\text{HT}$ generated by calcination at $100\text{ }^\circ\text{C}$ mainly afforded glycolic acid by a C-C bond cleavage of tartronic acid in the oxidation of glycerol in water solvent under an O_2 atmosphere (Scheme 5).¹¹¹ Calcination above $100\text{ }^\circ\text{C}$ provided a low active $\text{Au}_{\text{nano}}/\text{HT}$ catalyst owing to the aggregation of Au^0 particles. Zhang et al. recently reported the preferential deposition of Au nanoparticles with 2-3 nm diameter on the lateral $\{10\bar{1}0\}$ faces of the LDH large hexagonal crystals.¹¹² These Au nanoparticles are proposed to be responsible for the epoxidation of styrene to styrene oxide using *tert*-butyl hydroperoxide as an oxidant in benzene solvent.



Scheme 5 Oxidation pathway of glycerol

Platinum

HT-supported Pt nanoparticles ($\text{Pt}_{\text{nano}}/\text{HT}$) with mean diameter of 2.5 nm were highly active and selective reusable heterogeneous catalysts for base-free glycerol oxidation in pure water under an atmospheric O_2 pressure in a high glycerol/metal molar ratio up to 3125.¹¹³ High selectivity toward glyceric acid (GA: 78%) was achieved even at room temperature under air atmosphere (Scheme 5). The activity of the $\text{Pt}_{\text{nano}}/\text{HT}$ was greatly influenced by the HT Mg/Al ratio; glycerol conversion increased with increasing the HT Mg/Al ratio (from trace to 56%). The selectivity toward GA reached 70% when using the $\text{Pt}_{\text{nano}}/\text{HT}$ with Mg/Al ratio of 5 and 6. The $\text{Pt}_{\text{nano}}/\text{HT}$ was prepared by stirring the HT in aqueous solution of chloroplatinic acid hexahydrate ($\text{H}_2\text{PtCl}_6 \cdot 6\text{H}_2\text{O}$), followed by the reduction by aqueous formaldehyde at $100\text{ }^\circ\text{C}$. However, the Pt species was not completely reduced to zero valence state. The concentration of Pt^0 in the Pt nanoparticles is calculated by Pt L_{III} -edge XANES spectra. It was revealed that the glycerol conversion is proportional to the Pt^0 concentration, and more than 35% of Pt^0 was necessary for the selective oxidation.

Pt nanoparticles were prepared using soluble starch as a reducing and a stabilizing agent ($\text{Pt-starch}_{\text{nano}}$) and immobilized on the HT surface.¹¹⁴ The Pt mean particle size and the Pt^0

concentration can be controlled by reduction time (size: 0.9-2.1 nm, Pt⁰ concentration; 50-64%). The Pt-starch_{nano}/HT catalysts were applied for the oxidation of glycerol in water using an O₂. Pt particle size and the Pt⁰ concentration are proposed to be important factors in both glycerol conversion and GA yield in the glycerol oxidation. The Pt-starch_{nano}/HT was easily separated from the reaction mixture and recyclable for 3 times. When the Pt-starch_{nano}/HT was removed from the reaction mixture, no further oxidation proceeded.

Other metals (Cu, Mn, V, Ni, W, Rh)

The Cu⁰ nanoparticles with 7.5 nm mean diameter grafted on the HT surface (Cu_{nano}/HT) promote oxidant-free dehydrogenation of alcohols in *p*-xylene solvent.¹¹⁵ High-valent Mn species (average oxidation state; 6) can be created on the HT surface by the oxidation of Mn (average oxidation state; 3.1) using aqueous KOH solution at 40 °C.¹¹⁶ Smooth and reversible interconversion between low and high valence Mn cationic species enables the oxidation of benzylic alcohols to the corresponding carbonyl compounds using molecular oxygen at 100 °C in toluene solvent. This Mn-catalyzed alcohol oxidation may involve the radical pathway.

Choudary et al. found that the Ni^{II} species in the Brucite layer were active sites for the aerobic oxidation of benzylic and allylic alcohols in toluene solvent.¹¹⁷ The WO₄²⁻ species in the interlayer space promote the oxidation of substituted phenols with H₂O₂ to the corresponding *p*-quinol and *p*-quinol ethers with the aid of NH₄Br in a mixed solvent of EtOAc, MeOH, and water.¹¹⁸ The reaction of the WO₄²⁻ with H₂O₂ gives the W(O₂)_nO_{4-n}²⁻ as an active specie.

A monomeric tetrahedral V^V oxide species can be created on the HT surface, which efficiently catalyzes dehydration of amides to nitriles in mesitylene solvent.¹¹⁹ A monomeric Rh^{III} species grafted on the HT surface is found to promote heterogeneous 1,4-addition reaction of arylboronic acids to electron deficient olefins in 1,4-dioxane solvent.¹²⁰

The fine Ni and Cu nanoparticles can be formed on HT-derived materials. Ni_{nano}/Mg-Al mixed oxides,^{121,122} Cu_{nano}/ZnO/Al₂O₃^{123,124} and Cu_{nano}/Al₂O₃^{125,126} were prepared by calcination and reduction of Ni-containing HTs, co-precipitated Cu-Zn-Al HT and co-precipitated Cu-Al HT, respectively. These catalysts functioned as highly active and/or durable catalysts for methane steam reforming and CO shift reactions to produce hydrogen applicable for residential proton-exchange membrane fuel cell (PEMFC).

Metal-Metal Interactions

The catalytic activity of the HT-supported metals can be tuned by interactions between other metal species. The interaction between two metal species is strongly dependent on the location of the second metal.

Within the Brucite layer, Ru and Co cations can interact each other to enhance the oxidation

ability of the Ru cation sites (type (b), Figure 11).¹²⁷ It not only dehydrogenated various alcohols into the corresponding carbonyl compounds in toluene solvent but also oxygenated the benzylic positions of aromatic compounds, *i.e.* xanthene and fluorene, to give the corresponding ketones using atmospheric pressure of molecular oxygen even at 70 °C in chlorobenzene solvent. The Cu cation species in the Brucite layer can also work together with the surface Pd species to promote the reduction of nitrates in water solvent by H₂ at 20 °C.¹²⁸

The interaction between surface Ru cationic species and Mn ions was investigated in detail for the aerobic oxidation of benzyl alcohol in toluene solvent (Table 1).¹²⁹ The efficiency of the Ru species in the Brucite layer is not so high because most of Ru species are not exposed on the HT surface (entry 4) (type (b), Figure 11). The Ru species on the surface of the HT show higher catalytic activity than the layer-covered Ru cations (entry 3) (type (a) vs type (b), Figure 11). The interaction between surface Ru species and Mn cations in the Brucite layer enhances the activity (entry 2), however, to achieve complete benzyl alcohol conversion, 17-fold Mn cation (to Ru) is needed because the most of Mn cations in the Brucite layer do not interact with the surface Ru species. It was found that the interaction between surface Ru and Mn species is the most effective. To achieve 100% alcohol conversion, only 2-fold Mn cation is enough (entry 1) (type (a), Figure 11). Because the surface Mn species are completely inactive for the benzyl alcohol oxidation at 60 °C (entry 5), the formation of the RuMnMn trimetallic sites were proposed together with the results of the XAFS analysis. The neighboring Mn cation may accelerate the Ru-catalyzed alcohol oxidation by promoting the slow β-hydride elimination step of Ru-alcoholate intermediates.

Table 1 Aerobic oxidation of benzyl alcohol catalyzed by Ru-containing hydrotalcite catalysts.^a

entry	catalyst	conv.(%)	yield (%) ^b	Mn/Ru ratio
1	RuMn ₂ /Mg-Al-CO ₃	100	99	2
2	Ru/Mg-Mn-Al-CO ₃	100	99	17
3	Ru/Mg-Al-CO ₃	60	52	-
4	Mg-Al-Ru-CO ₃	13	10	-
5	Mn ₂ /Mg-Al-CO ₃	0	0	-

^a Reaction conditions: benzyl alcohol (1 mmol), catalyst (Ru: 3 mol%), toluene (5 mL), O₂ atmosphere, 60 °C, 1 h. ^b Yield of benzaldehyde.

The catalytic activity of Au nanoparticles with 2.7-3.9 nm supported on HT has been improved by addition of Cr(III) into the Brucite layer for the aerobic oxidation of benzylic and aliphatic alcohols in toluene solvent.¹³⁰ The promotion effect of Cr ion can be explained by the facilitated C-H bond

cleavage to produce the carbonyl compounds by surface chromium sites.

To control the metal-metal interactions in the active center, the poly(*N*-vinyl-2-pyrrolidone) (PVP)-protected bimetallic Au_xPd_y nanoclusters (Au_xPd_y-PVP_{nano}) with 2.6 nm particle size were immobilized on the HT surface and their activity was exploited for the aerobic oxidation of alcohols in toluene solvent.¹³¹ The Au₆₀Pd₄₀-PVP_{nano}/HT exhibited a significant catalytic activity for the alcohol oxidation, whereas the Pd₁₀₀-PVP_{nano}/HT and bare Au_{nano}/HT with the same particle sizes scarcely had oxidation activities under the same reaction condition. Notably, the prepared Au₆₀Pd₄₀-PVP_{nano}/HT catalyst showed the TON and TOF values for 395,700 and 69,100 h⁻¹, respectively in 250 mmol scale of 1-phenylethanol oxidation under solvent-free conditions. The XPS and Au *L*_{III}-edge XANES spectra indicated the presence of negatively charged Au sites in homogeneously-mixed AuPd alloy nanoparticle, which may explain the superiority of the Au₆₀Pd₄₀-PVP_{nano}/HT catalyst.

Very recently, Liu et al. reported that HT supported AuPd bimetallic catalyst promoted the C-C cross-coupling of primary and secondary benzylic alcohols in *p*-xylene solvent under N₂.¹³² It contains dehydrogenation of alcohols, aldol condensation, and transfer hydrogenation.

5. One-pot Synthesis Using Hydrotalcite Catalyst

One-pot reactions using heterogeneous catalysts afforded remarkably unique and environmentally-friendly benefits, including avoidance of isolation and purification of intermediate compounds, which save time, energy and solvent.¹³³ The concept of site isolation can be realized by the coexistence of acid and base without neutralization, which has been demonstrated using acid-base pairs of polymers, sol-gel matrices, and porous silicas.

Motokura et al. demonstrated the first example of one-pot reactions using two layered clays, HT as a solid base catalyst and titanium cation-exchanged montmorillonite (Ti⁴⁺-mont) as a solid acid catalyst (Figure 12).¹³⁴ Acid sites of Ti⁴⁺-mont are located within in the interlayer galley¹³⁵ whereas base sites of HT are exposed to the surface, led to avoidance of contact with catalytically active centers of each other. A combination of Ti⁴⁺-mont and HT afforded high conversion and product yield for a variety of acid-base reactions. One-pot synthesis of benzylidene malononitrile from malononitrile with benzaldehyde dimethyl acetal was successfully achieved in toluene solvent (>99% conversion of benzaldehyde dimethyl acetal and 93% yield of benzylidene malononitrile). This sequential reaction includes acid-catalyzed deacetalization and base-catalyzed aldol condensation. The system can be used for tandem Michael reaction and acetalization. Although conventional two-step synthesis gave less than 70% yield of a product, 2-methyl-2-(3-nitropropyl)-1,3-dioxalane from nitromethane, methyl vinyl ketone and ethane-1,2-diol, the one-pot system afforded 89% yield. Furthermore, one-pot synthesis of epoxy nitrile including four sequential reactions, namely esterification, deacetalization, aldol reaction

and epoxidation has been demonstrated in MeOH solvent as shown Scheme 6. A considerably high yield of epoxy nitrile (91%) has been obtained in a single reactor.

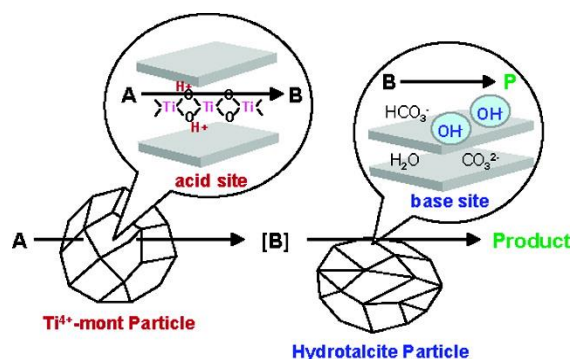
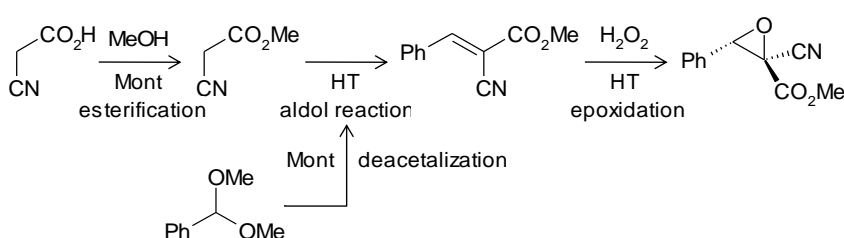


Figure 12 A one-pot reaction using titanium-cation exchanged montmorillonite and hydrotalcite.

[Reproduced with permission from American Chemical Society (ACS) of ref. 134]



Scheme 6 One-pot synthesis of epoxy nitrile from methanol, cyanoacetic acid, benzaldehyde dimethylacetal and H_2O_2 in four sequential acid and base reactions using Ti^{4+} -mont and hydrotalcite catalysts.

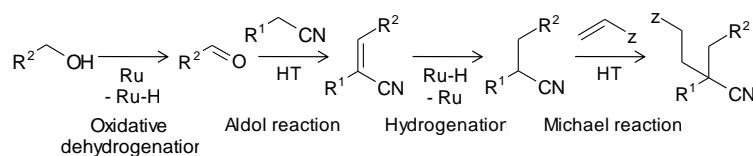
HTs can act as excellent supports for a variety of active metal nanoparticles (*vide supra*). This property is also very useful for one-pot reactions. Choudary et al. reported a one-pot synthesis of chiral diols which includes three different reactions using HT involving PdCl_4 , OsO_4 and WO_4 anions in a mixed solvent of *t*-BuOH and water.^{136,137} Three different reactions are (1) Mizoroki-Heck reaction by Pd species, (2) *N*-oxidation of *N*-methylmorpholine (NMM) toward *N*-methylmorpholine *N*-oxide (NMO) with hydrogen peroxide by W species, and (3) asymmetric dihydroxylation of olefins with NMM toward chiral diols by Os species (Scheme 7).



Scheme 7 The catalytic cycle in the LDH-PdOsW-catalyzed synthesis of chiral diols using H_2O_2 as the terminal oxidant. [Reproduced with permission from Wiley-VCH of ref. 136]

Motokura et al. also demonstrated several one-pot reactions using hydrotalcite-supported ruthenium catalyst (Ru/HT) and palladium nanoparticle catalyst ($\text{Pd}_{\text{nano}}/\text{HT}$).^{96,97,101,138} Owing to catalytic activity of metals and solid base catalysis, tandem reactions are successfully achieved. Ru/HT acted as an efficient catalyst for α -alkylation of nitriles with primary alcohols *via* metal-catalyzed oxidation and successive base-catalyzed aldol reaction in toluene solvent. This combination of alcohol oxidation and successive aldol reaction over the Ru/HT can be used for one-pot synthesis of quinolines from 2-aminobenzyl alcohol and various carbonyl compounds.¹³⁹

$\text{Pd}_{\text{nano}}/\text{HT}$ also is as an efficient solid catalyst for α -alkylation of nitriles with carbonyl compounds *via* aldol reaction and successive metal-catalyzed hydrogenation in toluene solvent. In addition, both Ru/HT and $\text{Pd}_{\text{nano}}/\text{HT}$ can produce glutaronitrile derivatives by Michael reaction of α -alkylated nitriles with electron-deficient olefins on the base sites of the HT after the metal/HT-catalyzed α -alkylation in a single reactor (Scheme 8). This tandem reaction includes four sequential reactions, oxidative dehydrogenation, aldol condensation, hydrogenation and Michael reaction.

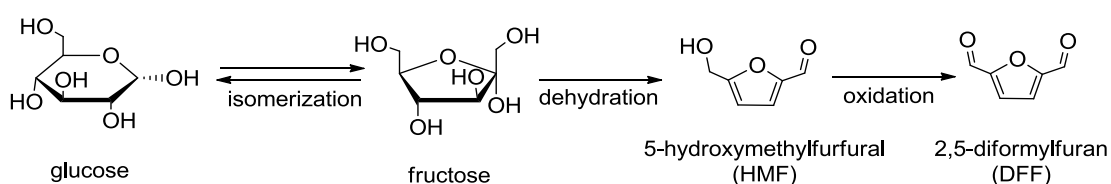


Scheme 8 Tandem reaction catalyzed by $\text{Ru}/\text{hydrotalcite}$

Application of one-pot reactions for biomass transformation has been studied.^{90,98,140-142} Furfurals including HMF and furfural are considered as very important intermediates for alternative fuels and chemicals. These furfurals are obtained from carbohydrates; the former is from hexoses such as

fructose, glucose and galactose, and the latter is from pentoses such as xylose and arabinose. In general, these furfurals are easily obtained from ketoses by removal of three water molecules (dehydration) in the presence of acid. For example, high yield and selectivity of HMF from fructose are achieved by using both homogeneous and heterogeneous acid catalysts. However, a direct synthesis of HMF and furfural from aldoses such as glucose and xylose is much more difficult although these aldoses are components of carbohydrate-based biomass (lignocellulose) and therefore widely available. In these regards, direct synthesis of furfurals from aldoses such as glucose and xylose has received much attention.

Takagaki et al. demonstrated a direct synthesis of HMF from glucose by using Mg-Al HT (solid base) and Amberlyst-15 (solid acid) in one-pot.^{90,140} The HT acts as a solid base catalyst for isomerization of glucose into fructose, and Amberlyst-15 as a solid acid for dehydration of fructose into HMF in DMF solvent. The combination of solid acid and base is very useful for a variety of furfurals production. This sequential reaction, (i) base-catalyzed aldose-ketose isomerization and (ii) acid-catalyzed dehydration of ketose, is successfully achieved for synthesis of HMF from glucose, galactose, furfural from xylose and arabinose, and 5-methyl-2-furaldehyde from rhamnose.^{90,140-142} Moreover, HMF can be directly produced from disaccharides such as cellobiose and sucrose in the presence of HT and Amberlyst-15. This one-pot reaction includes hydrolysis of disaccharides to monosaccharide by acid, isomerization by base and dehydration by acid. In addition, one-pot synthesis of 2,5-diformylfuran (DFF) which is dialdehyde formed by selective oxidation of HMF has demonstrated (Scheme 9).⁹⁸ DFF is obtained from glucose by using HT, Amberlyst-15 and the Ru/HT through three sequential reactions includes isomerization, dehydration and oxidation.



Scheme 9 One-pot synthesis of 2,5-diformylfuran (DFF) from glucose via fructose and 5-hydroxymethylfurfural (HMF).

Summary

The authors intended to overview recent advances of characterization, synthesis and liquid-phase catalysis of the layered hydrotalcite materials. A precise understanding of the structure and crystallization mechanism by advanced techniques leads to the highly-functionalized hydrotalcites as heterogeneous catalysts for pivotal reactions such as conversions of biomass-derived materials into

value-added chemicals.

Abbreviations

X@Y X-core coated by Y-shell (X, Y; element and/or compound(s))

Acknowledgements

The authors appreciate the Grant-in-Aid for Young Scientists (Start-up) (No. 20860038), Young Scientists (B) (No. 25820392) and Scientific Research (C) (No. 22560764) of the Ministry of Education, Culture, Sports, Science and Technology (MEXT), Japan. XAFS measurements for Pt_{nano}/HT, Cu_{nano}/Al₂O₃, Au_{nano}/HT and AuPd-PVP_{nano}/HT were performed at the BL01B1 of Spring-8 by the approval of the Japan Synchrotron Radiation Research Institute (JASRI) with proposal No. 2009B1497, 2009A1662 and 2009B1690, 2010A1598, and 2011A1607, respectively.

References

- 1 S. Miyata, *Clays Clay Miner.*, 1980, **28**, 50.
- 2 P. J. Sideris, U. G. Nielsen, Z. Gan and C. P. Grey, *Science*, 2008, **321**, 113.
- 3 F. Cavani, F. Trifirù and A. Vaccari, *Catal. Today*, 1991, **11**, 173.
- 4 B. F. Sels, D. E. De Vos, M. Buntinx, F. Pierard, A. Kirsch-De Mesmaeker and P. A. Jacobs, *Nature*, 1999, **400**, 855.
- 5 B. F. Sels, D. E. De Vos and P. A. Jacobs, *Catal. Rev. Sci. Eng.*, 2001, **43**, 443.
- 6 D. P. Debecker, E. M. Gaigneaux and G. Busca, *Chem. Eur. J.*, 2009, **15**, 3920-3935.
- 7 Y. Ono, H. Hattori, Solid Base Catalysis (eds A. W. Castleman, Jr., J. T. Toennis, K. Yamanouchi, W. Zinth) Springer Series in Chemical Physics 101, 2010, Tokyo Institute of Technology Press-Springer, Tokyo-Berlin.
- 8 P. J. Sideris, F. Blanc, Z. Gan and C. P. Grey, *Chem. Mater.*, 2012, **24**, 2449.
- 9 M. C. D. Mourad, M. Mokhtar, M. G. Tucker, E. R. Barney, R. I. Smith, A. O. Alyoubi, S. N. Basahel, M. S. P. Shaffer and N. T. Skipper, *J. Mater. Chem.*, 2011, **21**, 15479.
- 10 J. Zhang, Y. F. Xu, G. Qian, Z. P. Xu, C. Chen and Q. Liu, *J. Phys. Chem. C*, 2010, **114**, 10768.
- 11 M. B. J. Roefsaers, B. F. Sels, H. Uji-i, F. C. De Schryver, P. A. Jacobs and D. E. De Vos, *Nature*, 2006, **439**, 572.
- 12 K. Yu and J. R. Schmidt, *J. Phys. Chem. C*, 2011, **115**, 1887.
- 13 J. W. Boclair and P. S. Braterman, *Chem. Mater.*, 1999, **11**, 298.
- 14 J. W. Boclair and P. S. Braterman, J. Jiang, S. Lou, F. Yarberry, *Chem. Mater.*, 1999, **11**, 303.
- 15 W. J. McLaughlin, J. L. White and S. L. Hen, *J. Coll. Interface*, 1994, **165**, 41.
- 16 Z. P. Xu and G. Q. Lu, *Chem. Mater.*, 2005, **17**, 1055.
- 17 Y. Zhao, F. Li, R. Zhang, D. G. Evans and X. Duan, *Chem. Mater.*, 2002, **14**, 4286.
- 18 S. Abello and J. Perez-Ramirez, *Adv. Mater.*, 2006, **18**, 2436.
- 19 H. Takamura, J. Chiba, M. Ito, T. Takeda, S. Kikkawa, Y. Mawatari and M. Tabata, *J. Coll. Interface*, 2006, **300**, 648.
- 20 W. H. R. Shaw and J. Bordeaux, *J. Am. Chem. Soc.*, 1955, **77**, 4729.
- 21 U. Costantino, F. Marmottini, M. Nocchetti and R. Vivani, *Eur. J. Inorg. Chem.*, 1998, 1439.
- 22 J. M. Oh, S. Ho. Hwang and J. H. Choy, *Solid State Ionics*, 2002, **151**, 285.
- 23 Y. Yang, X. Zhao, Y. Zhu and F. Zhang, *Chem. Mater.*, 2012, **24**, 81.
- 24 Z. P. Xu, G. S. Stevenson, C. Q. Lu, G. Q. Lu, P. F. Bartlett and P. P. Gray, *J. Am. Chem. Soc.*, 2006, **128**, 36.
- 25 Q. Wang, H. H. Tay, Z. Guo, L. Chen, Y. Liu, J. Chang, Z. Zhong, J. Luo and A. Borgna, *Appl. Clay Sci.*, 2012, **55**, 18.
- 26 F. Winter, A. J. van Dillen and K. P. de Jong, *Chem. Commun.*, 2005, 3977.
- 27 L. Li and L. Shi, *Chem. Commun.*, 2008, 996.
- 28 E. Geraud, V. Prevot, J. Ghanbaja and F. Leroux, *Chem. Mater.*, 2006, **18**, 238.
- 29 E. Geraud, S. Rafqah, M. Sarakha, C. Forano, V. Prevot and F. Leroux, *Chem. Mater.*, 2008, **20**, 1116.

- 30 J. J. Woodford, J.-P. Dacquin, K. Wilson and A. F. Lee, *Energy Environ. Sci.*, 2012, **5**, 6145.
- 31 R. Ma, Z. Liu, L. Li, N. Iyi and T. Sasaki, *J. Mater. Chem.*, 2006, **16**, 3809.
- 32 S. Miyata, *Clays Clay Miner.*, 1983, **31**, 305.
- 33 N. Iyi, T. Matsumoto, Y. Kaneko and K. Kitamura, *Chem. Mater.*, 2004, **16**, 2926.
- 34 L. Li, R. Ma, Y. Ebina, N. Iyi and T. Sasaki, *Chem. Mater.*, 2005, **17**, 4386.
- 35 Z. Li, R. Ma, M. Osada, N. Iyi, Y. Ebina, K. Takada and T. Sasaki, *J. Am. Chem. Soc.*, 2006, **128**, 4872.
- 36 L. Li, Y. Feng, Y. Li, W. Zhao and J. Shi, *Angew. Chem. Int. Ed.*, 2009, **48**, 5888.
- 37 L. Li, R. Ma, N. Iyi, Y. Ebina, K. Takada and T. Sasaki, *Chem Commun.*, 2006, 3125.
- 38 D. Yan, J. Lu, M. Wei, J. Han, J. Ma, F. Li, X. Wang, D. G. Evans and X. Duan, *Angew. Chem. Int. Ed.*, 2009, **48**, 3073.
- 39 S. Komarneni, Q. H. Li and R. Roy, *J. Mater. Res.*, 1996, **11**, 1866.
- 40 P. Benito, F. M. Labajos and V. Rives, *Cryst. Growth Des.*, 2006, **6**, 1961.
- 41 P. Benito, F. M. Labajos, J. Rocha and V. Rives, *Micropor. Mesopor. Mater.*, 2006, **94**, 148.
- 42 P. Benito, M. Herrero, F. M. Labajos and V. Rives, *Appl. Clay Sci.*, 2010, **48**, 218.
- 43 O. Bergada, I. Vicente, P. Salagre, Y. Cesteros, F. Medina and J. E. Sueiras, *Micropor. Mesopor. Mater.*, 2007, **101**, 363.
- 44 D. Tichit, A. Rolland, F. Prinetto, G. Fetter, M. de J. Martinez-Ortiz, M. A. Valenzuela and P. Bosch, *J. Mater. Chem.*, 2002, **12**, 3832.
- 45 M. J. Climent, A. Corma, S. Iborra, K. Epping and A. Velty, *J. Catal.*, 2004, **225**, 316.
- 46 J. A. Rivera, G. Fetter and P. Bosch, *Microp. Mesop. Mater.*, 2006, **89**, 306.
- 47 W. N. Budhysutanto, F. J. Van Den Bruele, B. D. Rossenaar, D. Van Agterveld, W. J. P. Van Enckevort and H. J. M. Kramer, *J. Cryst. Growth*, 2011, **318**, 110.
- 48 J. H. Choy, S. Y. Kwak, Y. J. Jeong and J. S. Park, *Angew. Chem. Int. Ed.*, 2000, **39**, 4041
- 49 H. Zhang, R. Qi, D. G. Evans and X. Duan, *J. Solid State Chem.*, 2004, **177**, 772.
- 50 Y. Xu, H. Zhang, X. Duan and Y. Ding, *Mater. Chem. Phys.*, 2009, **114**, 795.
- 51 S. Nishimura, A. Takagaki and K. Ebitani, *Bull. Chem. Soc. Jpn.*, 2010, **83**, 846.
- 52 D. Pan, H. Zhang, T. Fan, J. Chen and X. Duan, *Chem. Commun.*, 2011, **47**, 908.
- 53 F. Mai, X. Chen, Y. Ma, S. Yin, F. Yuan and H. Zhang, *Chem. Commun.*, 2011, **47**, 12804.
- 54 M. Shao, F. Ning, J. Zhao, M. Wei, D. G. Evens and X. Due, *J. Am. Chem. Soc.*, 2012, **134**, 1071.
- 55 C. Chen, P. Gunawan, X. W. Lou and R. Xu, *Adv. Funct. Mater.*, 2012, **22**, 780.
- 56 J. Liu, Y. Li, X. Huang, G. Li and Z. Li, *Adv. Funct. Mater.*, 2008, **18**, 1448.
- 57 S. Nishimura, A. Takagaki and K. Ebitani, unpublished data.
- 58 J. X. He, S. Yamashita, W. Jones and A. Yamaguchi, *Langmuir*, 2002, **18**, 1580.
- 59 A. S. Costa and T. Imae, *Langmuir*, 2004, **20**, 8865.
- 60 F. Zhang, M. Sun, S. Xu, L. Zhao and B. Zhang, *Chem. Eng. J.*, 2008, **141**, 362.
- 61 H. Chen, F. Zhang, S. Fu and X. Duan, *Adv. Mater.*, 2006, **18**, 3089.
- 62 F. Zhang, L. Zhao, H. Chen, S. Xu, D. G. Evans and X. Duan, *Angew. Chem. Int. Ed.*, 2008, **47**, 2466.
- 63 J. H. Lee, S. W. Rhee and D. Y. Jung, *J. Am. Chem. Soc.*, 2007, **129**, 3522.

- 64 J. H. Lee, S. W. Rhee, H. J. Nam and D. Y. Jung, *Adv. Mater.*, 2009, **21**, 546.
- 65 D. Yan, J. Lu, J. Ma, M. Wei, X. Wang, D. G. Evans and X. Duan, *Langmuir*, 2010, **26**, 7007.
- 66 B. M. Choudary, M. L. Kantam, B. Kavita, Ch. V. Reddy, K. K. Rao and F. Figueras, *Tetrahedron Lett.*, 1998, **39**, 3555.
- 67 T. Honma, M. Nakajo, T. Mizugaki, K. Ebitani and K. Kaneda, *Tetrahedron Lett.*, 2002, **43**, 6229.
- 68 S. Ueno, K. Yamaguchi, K. Yoshida, K. Ebitani and K. Kaneda, *Chem. Commun.*, 1998, 295.
- 69 K. Yamaguchi, K. Ebitani and K. Kaneda, *J. Org. Chem.*, 1999, **64**, 2966.
- 70 K. Kaneda and S. Ueno, 1996, 300, ACS Symposium Series 638, Heterogeneous Hydrocarbon Oxidation, eds., B. K. Warren and S. T. Oyama, American Chemical Society.
- 71 D. G. Cantrell, L. J. Gillie, A. F. Lee and K. Wilson, *Appl. Catal. A: Gen.*, 2005, **287**, 183.
- 72 Y. Xi and R. J. Davis, *J. Catal.*, 2008, **254**, 190.
- 73 Y. Xi and R. J. Davis, *J. Catal.*, 2009, **268**, 307.
- 74 L. Gao, G. Teng, J. Lv and G. Xiao, *Energy Fuels*, 2010, **24**, 646.
- 75 Y. Xiao, L. Gao, G. Xiao, B. Fu and L. Niu, *Ind. Eng. Chem. Res.*, 2012, **51**, 11860.
- 76 M. J. Campos-Molina, J. Santamaria-Gonzalez, J. Merida-Robles, R. Moreno-Tost, M. C. G. Albuquerque, S. Bruque-Gamez, E. Rodriguez-Castellon, A. Jimenez-Lopez and P. Maireles-Torres, *Energy Fuels*, 2010, **24**, 979.
- 77 W. Xie, Y. Liu and H. Chun, *Catal. Lett.*, 2012, **142**, 352.
- 78 M. Kouzu, T. Kasuno, M. Tajika, S. Yamanaka and J. Hidaka, *Appl. Catal. A: Gen.*, 2008, **334**, 357
- 79 M. L. Granados, D. M. Alonso, I. Sadaba, R. Mariscal and P. Ocon, *Appl. Catal. B: Environ.*, 2009, **89**, 265.
- 80 F. S. H. Simanjuntak, T. K. Kim, S. D. Lee, B. S. Ahn, H. S. Kim and H. Lee, *Appl. Catal. A: Gen.*, 2011, **401**, 220.
- 81 O. Meyer, F. Roessner, R. A. Rakoczy and R. W. Fischer, *ChemCatChem*, 2010, **2**, 314.
- 82 A. Takagaki, K. Iwatani, S. Nishimura and K. Ebitani, *Green Chem.*, 2010, **12**, 578.
- 83 A. Kumar, K. Iwatani, S. Nishimura, A. Takagaki and K. Ebitani, *Catal. Today*, 2012, **185**, 241.
- 84 M. G. Alvarez, M. Pliskova, A. M. Segarra, F. Medina and F. Figueras, *Appl. Catal. B: Env.*, 2012, **113-114**, 212.
- 85 M. G. Alvarez, R. J. Chimentao, F. Figueras and F. Media, *Appl. Clay Sci.*, 2012, **58**, 16.
- 86 M. G. Alvarez, A. M. Segarra, S. Contreras, J. E. Sueriras, F. Medina and F. Figueras, *Chem. Eng. J.*, 2010, **161**, 340.
- 87 M. J. Climent, A. Corma, P. D. Frutos, S. Iborra, M. Noy, A. Velty and P. Concepcion, *J. Catal.*, 2010, **269**, 140.
- 88 For example, M. Moliner, Y. Román-Leshkov and M. E. Davis, *PNAS*, 2010, **207**, 6164.
- 89 C. Moreau, R. Durand, A. Roux and D. Tichit, *Appl. Catal. A: Gen.*, 2000, **193**, 257.
- 90 A. Takagaki, M. Ohara, S. Nishimura and K. Ebitani, *Chem. Commun.*, 2009, 6276.
- 91 S. Yu, E. Kim, S. Pak, I. K. Song and J. C. Jung, *Catal. Commun.*, 2012, **29**, 63.
- 92 K. Ebitani, K. Motokura, K. Mori, T. Mizugaki and K. Kaneda, *J. Org. Chem.*, 2006, **71**, 5440.
- 93 It should be noted that the modified basicity of reconstructed hydrotalcite was observed only

when the calcination and hydration were performed under a flow of inert gas. An exposure to air should be avoided because of the CO₂ adsorption onto the surface base sites.

- 94 A. Lemos and J. Lourenço, *Arkivoc*, 2010, 170.
- 95 K. Kaneda, T. Yamashita, T. Matsushita, K. Ebitani, *J. Org. Chem.*, 1998, **63**, 1750.
- 96 K. Motokura, D. Nishimura, K. Mori, T. Mizugaki, K. Ebitani and K. Kaneda, *J. Am. Chem. Soc.*, 2004, **126**, 5662.
- 97 K. Motokura, N. Fujita, K. Mori, T. Mizugaki, K. Ebitani, K. Jitukawa and K. Kaneda, *Chem. Eur. J.*, 2006, **12**, 8228.
- 98 A. Takagaki, M. Takahashi, S. Nishimura and K. Ebitani, *ACS Catal.*, 2011, **1**, 1562.
- 99 D. Saumya, S. Nishimura and K. Ebitani, submitted for publication.
- 100 N. Kakiuchi, Y. Maeda, T. Nishimura and S. Uemura, *J. Org. Chem.*, 2001, **66**, 6620.
- 101 K. Motokura, N. Fujita, K. Mori, T. Mizugaki, K. Ebitani and K. Kaneda, *Tetrahedron Lett.*, 2005, **46**, 5507.
- 102 T. Mitsudome, Y. Mikami, H. Funai, T. Mizugaki, K. Jitsukawa and K. Kaneda, *Angew. Chem. Int. Ed.*, 2008, **47**, 138.
- 103 M. Haruta, *CATTECH*, 2002, **6**, 102.
- 104 J. Huang, T. Akita, J. Faye, T. Fujitani, T. Takei and M. Haruta, *Angew. Chem. Int. Ed.*, 2009, **48**, 7862.
- 105 T. Mitsudome, A. Noujima, T. Mizugaki, K. Jitsukawa and K. Kaneda, *Green Chem.*, 2009, **11**, 793.
- 106 T. Mitsudome, A. Noujima, Y. Mikami, T. Mizugaki, K. Jitsukawa and K. Kaneda, *Angew. Chem. Int. Ed.*, 2010, **49**, 5545.
- 107 A. Noujima, T. Mitsudome, T. Mizugaki, K. Jitsukawa and K. Kaneda, *Angew. Chem. Int. Ed.*, 2011, **50**, 2986.
- 108 A. Noujima, T. Mitsudome, T. Mizugaki, K. Jitsukawa and K. Kaneda, *Chem. Commun.*, 2012, **48**, 6723.
- 109 W. Fang, Q. Zhang, J. Chen, W. Deng and Y. Wang, *Chem. Commun.*, 2010, **46**, 1547.
- 110 N. K. Gupta, S. Nishimura, A. Takagaki and K. Ebitani, *Green Chem.*, 2011, **13**, 824.
- 111 A. Takagaki, A. Tsuji, S. Nishimura and K. Ebitani, *Chem. Lett.*, 2011, **40**, 150.
- 112 F. Zhang, X. Zhao, C. Feng, B. Li, T. Chen, W. Lu, X. Lei and S. Xu, *ACS Catal.*, 2011, **1**, 232.
- 113 A. Tsuji, K. T. V. Rao, S. Nishimura, A. Takagaki and K. Ebitani, *ChemSusChem*, 2011, **4**, 542.
- 114 D. Tongsakul, S. Nishimura, C. Thammacharoen, S. Ekgasit and K. Ebitani, *Ind. Eng. Chem. Res.*, 2012, **51**, 16182.
- 115 T. Mitsudome, Y. Mikami, K. Ebata, T. Mizugaki, K. Jitsukawa and K. Kaneda, *Chem. Commun.*, 2008, 4804.
- 116 K. Nagashima, T. Mitsudome, T. Mizugaki, K. Jitsukawa and K. Kaneda, *Green Chem.*, 2010, **12**, 2142.
- 117 B. M. Choudary, M. L. Kantam, A. Rahman, Ch. V. Reddy and K. K. Rao, *Angew. Chem. Int. Ed.*, 2001, **40**, 763.
- 118 B. F. Sels, D. E. De Vos and P. A. Jacobs, *Angew. Chem. Int. Ed.*, 2005, **44**, 310.

- 119 S. Sueoka, T. Mitsudome, T. Mizugaki, K. Jitsukawa and K. Kaneda, *Chem. Commun.*, 2010, **46**, 8243.
- 120 K. Motokura, N. Hashimoto, T. Hara, T. Mitsudome, T. Mizugaki, K. Jitsukawa and K. Kaneda, *Green Chem.*, 2011, **13**, 2416.
- 121 K. Takehira, T. Shishido, P. Wang, T. Kosaka and K. Takai, *Phys. Chem. Chem. Phys.*, 2003, **5**, 3801.
- 122 K. Takehira, T. Kawabata, T. Shishido, K. Murakami, T. Ohi, D. Shoro, M. Honda and K. Takaki, *J. Catal.*, 2005, **231**, 92.
- 123 T. Shishido, Y. Yamamoto, H. Morioka, K. Takai and K. Takehira, *Appl. Catal. A: Gen.*, 2004, **263**, 249.
- 124 T. Shishido, M. Yamamoto, D. Li, Y. Tian, H. Morioka, M. Honda, T. Sano and K. Takehira, *Appl. Catal. A: Gen.*, 2006, **303**, 62.
- 125 S. Nishimura, T. Shishido, K. Ebitani, K. Teramura and T. Tanaka., *Appl. Catal. A: Gen.*, 2010, **387**, 185.
- 126 S. Nishimura, T. Shishido, J. Ohyama, K. Teramura, A. Takagaki, T. Tanaka and K. Ebitani, *Catal. Sci. Technol.*, 2012, **2**, 1685.
- 127 T. Matsushita, K. Ebitani and K. Kaneda, *Chem. Commun.* 1999, 265.
- 128 A. E. Palomares, J. G. Prato, F. Rey and A. Corma, *J. Catal.*, 2004, **221**, 62.
- 129 K. Ebitani, K. Motokura, T. Mizugaki and K. Kaneda, *Angew. Chem. Int. Ed.*, 2005, **44**, 3423.
- 130 P. Liu, Y. Guan, R. A. van Santen, C. Li and E. J. M. Hensen, *Chem. Commun.*, 2011, **47**, 11540.
- 131 S. Nishimura, Y. Yakita, M. Katayama, K. Higashimine and K. Ebitani, *Catal. Sci. Technol.*, 2013, **3**, 351.
- 132 X. Liu, R-S. Ding, L. He, Y-M. Liu, Y. Cao, H-Y. He and K-N. Fan, *ChemSusChem*, 2013, **6**, 604.
- 133 B. Voit, *Angew. Chem. Int. Ed.*, 2006, **45**, 4238.
- 134 K. Motokura, N. Fujita, K. Mori, T. Mizugaki, K. Ebitani and K. Kaneda, *J. Am. Chem. Soc.*, 2005, **127**, 9674.
- 135 K. Ebitani, T. Kawabata, K. Nagashima, T. Mizugaki and K. Kaneda, *Green Chem.*, 2000, **2**, 157.
- 136 B. M. Choudary, N. S. Chowdari, S. Madhi and M. L. Kantam, *Angew. Chem. Int. Ed.*, 2001, **40**, 4619.
- 137 B. M. Choudary, N. S. Chowdari, S. Madhi and M. L. Kantam, *J. Org. Chem.*, 2003, **68**, 1736.
- 138 K. Kaneda, K. Jitsukawa, K. Ebitani, T. Mizugaki, K. Motokura, *Res. Chem. Intermed.*, 2008, **34**, 475.
- 139 K. Motokura, T. Mizugaki, K. Ebitani and K. Kaneda, *Tetrahedron Lett.*, 2004, **45**, 6029.
- 140 M. Ohara, A. Takagaki, S. Nishimura and K. Ebitani, *Appl. Catal. A*, 2010, **373**, 149.
- 141 A. Takagaki, M. Ohara, S. Nishimura and K. Ebitani, *Chem. Lett.*, 2010, **39**, 838.
- 142 J. Tuteja, S. Nishimura and K. Ebitani, *Bull. Chem. Soc. Jpn.*, 2012, **85**, 275.